Redox Biology 57 (2022) 102494

Contents lists available at ScienceDirect

Redox Biology

journal homepage: www.elsevier.com/locate/redox

Lycopene attenuates the inflammation and apoptosis in aristolochic acid nephropathy by targeting the Nrf2 antioxidant system

Yu Wang [a], Zhihui Liu [a], Jun Ma [a], Qingyang Xv [a], Hongxin Gao [a], Hang Yin [a], Ge Yan [a], Xiaowen Jiang [a,*], Wenhui Yu [a,b,c,**]

[a] Department of Veterinary Medicine, Northeast Agricultural University, Harbin, 150030, China
[b] Heilongjiang Provincial Key Laboratory for Prevention and Control of Common Animal Diseases, Northeast Agricultural University, Harbin, 150030, China
[c] Institute of Chinese Veterinary Medicine, Northeast Agricultural University, Harbin, 150030, China

ARTICLE INFO

Keywords:
Lycopene
Aristolochic acid nephropathy
Oxidative stress injury
Inflammatory response
Apoptosis
Nrf2/HO-1 signaling pathway

ABSTRACT

Lycopene (LYC) is a carotenoid, has antioxidant properties. This study investigated whether lycopene attenuates aristolochic acids (AAs) -induced chronic kidney disease. In this experiment, lycopene was used to intervene C57BL/6 mice with renal injury induced by aristolochic acid exposure. The histomorphological changes and serological parameters of the kidney were measured in order to assess the alleviating effect of lycopene on renal injury in aristolochic acid nephropathy. In vitro and in vivo experiments were carried out to verify the main mechanism of action and drug targets of lycopene in improving aristolochic acid nephropathy (AAN) and by various experimental methods such as ELISA, immunohistochemistry, immunofluorescence, Western-blot and qRT-PCR. The results showed that oxidative stress injury was induced in the kidney of mice after AAI exposure, resulting in inflammatory response and tubular epithelial cell apoptosis. The results showed that the Nrf2/HO-1 antioxidant signaling pathway was inhibited after AAI exposure. AAI induces oxidative stress injury in the kidney, which ultimately leads to inflammation and tubular epithelial cell apoptosis. After LYC intervened in the body, it activated Nrf2 nuclear translocation and its downstream HO-1 and NQO1 antioxidant signaling pathways. LYC inhibited ROS production by renal tubular epithelial cells, and alleviated mitochondrial damage. LYC further modulated the TNF-α/NF-κB signaling cascade, thereby reduced the accumulation of inflammatory factors in the renal interstitium. Moreover, LYC was able to up-regulate the expression of Bcl-2, down-regulate Bax expression and inhibit the activation of cleaved forms of Caspase-9 and Caspase-3, which finally attenuated the apoptosis of the mitochondrial pathway induced by AAI exposure. It was concluded that lycopene was able to activate the Nrf2 antioxidant signaling pathway to maintain the homeostasis of renal oxidative stress and ultimately attenuated renal inflammatory response and apoptosis. These results suggested that lycopene can be used as a drug to relieve AAN.

1. Introduction

Aristolochic acids (AAs) are a general term for a class of nitrobenzoic acid compounds, which are widespread in Aristolochic and Asarum plants in a variety of structural forms. Since the 1990s, an unusual renal disease composed of progressive tubulointerstitial nephritis has been first identified in young Belgian female patients after taking aristolochic acid [1]. AAN has attracted much attention from the international medical community. Aristolochic acid nephropathy is a chronic kidney disease (CKD) that is transformed from acute kidney injury (AKI) and is mainly pathologically characterized by extensive tubulointerstitial fibrosis with tubular atrophy and loss. The decline in glomerular filtration rate and retention of uremic solutes are the main reasons why CKD is difficult to treat [2]. At present, CKD has become an important

Abbreviations: AAI, Aristolochic acid I; LYC, Lycopene; AAN, Aristolochic acid nephropathy; Nrf2, Nuclear factor erythroid 2-related factor 2; HO-1, Heme oxygenase-1; KEAP-1, Kelch-like ECH-associated protein 1; BAX, Bcl-2-like protein 4; BCL-2, B cell lymphoma/lewkmia-2; T-AOC, Total antioxidant capacity; SOD, Superoxide Dismutase; MDA, Malondialdehyde; ROS, Reactive oxygen species; TNF-α, Tumor necrosis factor-alpha; NQO1, NAD(P)H dehydrogenase [quinone] 1.

* Corresponding author.
** Corresponding author. Heilongjiang Provincial Key Laboratory for Prevention and Control of Common Animal Diseases, Northeast Agricultural University, Harbin, 150030, China.
E-mail addresses: 345915159@qq.com (Y. Wang), jiangxiaowen@neau.edu.cn (X. Jiang), yuwenhui@neau.edu.cn (W. Yu).

https://doi.org/10.1016/j.redox.2022.102494
Received 6 September 2022; Received in revised form 26 September 2022; Accepted 27 September 2022
Available online 28 September 2022

health problem of common concern all over the world. The prevalence of CKD is expected to increase as new reliable therapies have not been identified. Therefore, the first step is to treat this chronic kidney disease by controlling acute kidney injury (AKI). The main manifestation of AKI is a sharp decline in renal function. Current studies have shown that the pathogenesis of AKI includes renal vein congestion, inflammatory response [3,4], oxidative stress, activation of coagulation cascade, renal hypoperfusion and microcirculatory disturbance [5]. It has been shown that AAI acts on the body's antioxidant enzyme system to make antioxidant dysfunction abnormal, ultimately leading to mitochondrial damage [6]. In addition, studies have demonstrated that AAI can promote the activation of P53 and Caspase-3 to cause apoptosis, which in turn induces progressive tubular atrophy with tubular epithelial cell regeneration defects [7]. Jiafa Ren et al. showed in their study that deletion of Twist1 in the distal nephron was able to attenuate renal damage, interstitial fibrosis, renal inflammation and susceptibility to apoptosis after aristolochic acid exposure [8].

Oxidative stress damage is caused when the production of oxidative metabolites in the body increases or the protective mechanisms of the intracellular antioxidant system change [9]. ROS are mediators of intracellular signaling cascades [10], and release of large amounts of free radicals when they are relatively excessive exerts toxic effects. Accumulation of ROS is able to trigger various diseases such as inflammatory response, growth arrest and cell death [11–13]. Nuclear factor (erythroid-derived 2) -like 2 (NFE2L2, also known as Nrf2) is an important regulator in the antioxidant system and is involved in regulating intracellular redox homeostasis, heavy metal disconnection, inflammatory responses, and the metabolism of a variety of electrophilic substances [14]. It has been shown that the Nrf2/heme oxygenase-1 (HO-1) signaling pathway is one of the most important antioxidant defense mechanisms in the body [15]. Nrf2 has attracted great interest as a therapeutic target for renal fibrosis and chronic kidney disease. It has been shown that the Nrf2-HO-1 antioxidant system is able to resist cyclosporine-induced renal fibrosis in mice [16]. When ROS are overproduced and overaccumulated, they are able to activate nuclear factor κB (NF-κB) and its nuclear receptors. NF-κB is a transcription factor whose complex includes five members: RelA (p65), RelB, c-Rel, NF-κB1 (p50), and NF-κB2 (p52). NF-κB plays an important function in immune response and cell survival by targeting proinflammatory genes [17]. Previous studies have demonstrated that NF-κB is able to regulate the transcription of apoptosis-related genes (Bax and Bcl-2) and cell proliferation regulators [cyclooxygenase-2 (COX-2)] during tumorigenesis [18]. And it can activate the expression of NF-κB/NLRP3/IL-1β inflammation-related pathways when the body develops an inflammatory response. This in turn induces the production and accumulation of ROS ultimately leading to abnormal antioxidant function in the body [81].

Lycopene (LYC) is a carotenoid compound found in red fruits and vegetables such as tomatoes, papaya, pink grapefruit, and watermelon [19]. LYC can scavenge excess monooxygen and free radicals in the body, which is a highly effective antioxidant [20]. For a long time, the pharmacological action and clinical development of lycopene have been the research hotspots in the field of pharmacy at home and abroad. It has been confirmed that lycopene has antioxidant [21], anti-inflammatory [22,23], anti-apoptotic and anti-cancer [24] effects and can correct metabolic syndrome and liver injury in diet-induced obese rats through anti-fibrotic pathways [25]. In previous studies, it was demonstrated that lycopene is able to activate the nuclear translocation of Nrf2 and antioxidant system which in turn inhibits oxidative stress to prevent liver injury induced by plasticizer (DEHP) in mice [26]. Lycopene decreased NF-κB and Cox-2 protein expression and inhibited inflammatory factor expression in the esophageal tissue of F344 esophageal cancer rats [27]. Although many functions of lycopene have been demonstrated, whether lycopene can ameliorate nephrotoxicity induced by AAI and its specific protective mechanism has not been reported. Therefore, the aim of this study was to explore whether lycopene intervention was able to attenuate AAI exposure-induced nephrotoxicity. Whether its mechanism of action is related to inhibition of oxidative stress injury, inflammatory response, and apoptosis, as well as verification of the relationship between the Nrf2 antioxidant system and TNF-α/NF-κB inflammatory signaling pathway, apoptosis of the mitochondrial pathway.

2. Materials and methods

2.1. Determination of AA-I and lycopene in rat kidney by HPLC

Thirty-three 8-week-old healthy adult male SD rats (200 g ± 20 g) were purchased from Liaoning Changsheng Biotechnology Co., Ltd. Adaptive housing for one week prior to the formal start of the experiment. The housing conditions for the mice were set at a temperature of 21–23 °C, a relative humidity of 35%–65%, and a 12-h light/dark cycle.

33 healthy male SD rats were divided into 3 groups：control group (Con), AAI group, AAI + LYC group. Blank group consisted of 6 rats. Twenty-seven rats in the AAI group were intragastrically administered with AAI. Twenty-seven rats in the AAI + LYC group were intragastrically administered with AAI and LYC. Each mouse was dosed once. Three rats were randomly dissected at each time point of 0.25 h/0.5 h/1 h/2 h/4 h/8 h/12 h/24 h/48 h after administration. Subsequently, the kidneys were pretreated and the concentration of AAI and lycopene in renal tissue was measured by HPLC.

Detection of AAI content in kidney: 0.3 ～ 1g kidney tissues were taken, added with normal saline at 1:3 (W: V) for grinding to prepare tissue homogenate. 100 μL of tissue homogenate was acidified with 100 μL of 2 mol/L HCL. Vortex mix for 10s and then add 50 times 95% ethanol and vortex mix for 3 min. The resulting liquid was centrifuged at 8000 r/min for 15 min and the supernatant recovered. The supernatant was dried in a vacuum oven at 45 °C. The resulting residue was sonicated with 2 mL of methanol and passed through a 0.22 μm membrane. Finally, 20 μL was taken for HPLC analysis. Chromatographic conditions: The chromatographic column was DiKMAC18 (2.1 mm × 50 mm, 5 μm, Dima Technology Co., Ltd.); Mobile phase: methanol : water : glacial acetic acid (70:29.5:0.5, V/V/V); Detection wavelength: 390 nm; Column temperature: 25 °C; Injection volume: 20 μL.

Detection of lycopene content in kidney: Weighed 0.5 g kidney tissue was ground into tissue homogenate after adding 1 ml normal saline. Protein was subsequently precipitated by adding 100 μL of absolute ethanol to 100 μL of tissue homogenate. Then 200 μL of n-hexane (containing 0.01% BHT) was added. The mixture was vortexed for 1 min and centrifuged at 4000 rpm for 6 min to collect the supernatant. All supernatants were combined after repeated extraction of the pellet. Evaporate the supernatant to dryness under nitrogen using a nitrogen blow apparatus. The residue was then reconstituted in 100 μL dichloromethane. Samples were then filtered with a 0.22 μm membrane for HPLC analysis [80,82]. Chromatographic conditions: HPLC was used to determine the quantification of the isolated DHS. A Shimadzu HPLC system equipped with an LC-10ATVP binary pump, SPD-10AVP detector, CTO-10ASVP columnoven,and N300 workstation was employed for analysis. A C18 column·(150 mm × 4.6 mm , 5 μm Diamonsil, Dikma Technologies, China) was used for the separation of the compounds. Mobile phase ratio (Methanol: Acetonitrile: Dichloromethane = 50:33:17, V/V/V); Detection wavelength: 472 nm; Column temperature: 25 °C; Injection volume: 10 μL.

2.1.1. Animal experiment and group administration

All animal experiments were approved by the Animal Ethics Committee of Northeast Agricultural University. SPF grade C57BL/6 male mice aged 6 weeks and weighing (18 g–20 g). Standard diet for SPF grade mouse growth and breed were purchased from Liaoning Changsheng Biotechnology Co., Ltd. (Benxi, Liaoning, China). Adaptive housing for one week prior to the formal start of the experiment. The housing conditions for the mice were set at a temperature of 21–23 °C, a

Table 1
Animal groups.

Groups	Treatment (8:00am)	Treatment (13:00pm)
Group 1 (Con)	0.5%CMC	0.5%CMC
Group 2 (AAN)	0.5%CMC	AAI (10 mg/kg BW1/day)
Group 3(LYC)	LYC (20 mg/kg BW1/day)	0.5%CMC
Group 4(AL5)	LYC (5 mg/kg BW1/day)	AAI (10 mg/kg BW1/day)
Group 5 (AL20)	LYC (20 mg/kg BW1/day)	AAI (10 mg/kg BW1/day)

relative humidity of 35%–65%, and a 12-h light/dark cycle.

The experimental mice were randomly divided into the following five groups (6 mice/group): control group (Con), model group (AAN), LYC control group (20 mg/kg/d) (LYC), low dose LYC treatment group (5 mg/kg/d) (AL5), and high dose LYC treatment group (20 mg/kg/d) (AL20). Intragastric administration for 28 days. The administration dose of aristolochic acid was based on the results of preliminary experiment in this experiment. Compared with the normal control group, when the administration concentration of AAI reached 10 mg/kg/day, the results of HE staining and Masson staining showed severe tubular injury, significant fibrosis in the kidney, and significantly increased the contents of CR and BUN in the serum (Supplementary Fig. 1). The administration dose of LYC was based on the previous study and report [28]. The administration dose is shown in Table 1. Animal experimental procedure is shown in Fig. 3-A.

2.2. Determination of renal coefficient and histopathological observation

Twenty-four hours after the last administration, the mice were sacrificed and serum and organs were collected. The kidneys were photographed and weighed, and the kidney coefficient (ratio between kidney and mouse body weight) was calculated. Renal tissues were made into pathological sections and stained with HE (hematoxylin and eosin), periodic acid-Schiff staining (PAS) and Masson staining [29].

Renal histopathology was scored as follows: (a) presence of crescents or fibrosis in glomeruli (1%–10%, grade 1; 10%–25%, grade 2; 25%–50%, grade 3; >50%, grade 4); (b) tubular cell changes (1%–10%, grade 1; 10%–25%, grade 2; 25%–50%, grade 3; >50%, grade 4); (c) lymphocytic infiltrates (1%–10%, grade 1; 10%–25%, grade 2; 25%–50%, grade 3; >50%, grade 4); (d) vasculitis (grade 1, small but well-defined perivascular infiltrates; grade 2, 1–3 perivascular infiltrates, no necrosis; grade 3, 3–5 perivascular infiltrates, more extensive; grade 4, more than 5 perivascular infiltrates) based on the results of HE staining. The sum of the four histopathological scores was calculated [30].

Renal injury was scored based on the results of PAS staining. Scoring was based on tubular dilatation, cast formation, tubular atrophy, absence of brush border. The grade of renal injury was based on a semi-quantitative score to grade the degree of tubular injury [31]. Tissue damage was examined in a blinded fashion and scored according to the percentage of injured tubules: 0: no injury; 1: <25%; 2: 25%–50%; 3: 50%–75%; 4: >75% [32].

2.3. Determination of renal function and oxidative stress markers

Blood samples were centrifuged at room temperature to collect serum. The contents of creatinine (Cr) (C011-2-1) and blood urea nitrogen (BUN) (C013-2-1) in serum were measured using a commercial kit from Nanjing Jiancheng Bioengineering (Nanjing, China) to indicate renal function [33]; the contents of malondialdehyde (MDA) (A003-1-2) and peroxidase (SOD) (A001-3-2) in mouse renal tissue and the activities of total antioxidant capacity (T-AOC) (A015-2-1) and glutathione peroxidase (GSH-PX) (A005-1-2) were measured to indicate oxidative stress levels [34].

2.4. Immunohistochemical detection of Nrf2/NF-kB

Sections of 5 μm thick kidney tissue were deparaffinized using xylene and rehydrated in graded alcohols. Non-specific epitopes were blocked with rabbit serum over 30 min and subsequently incubated with primary antibodies against Nrf2 (1:200) and NF-kB (1:400) in a humidified chamber overnight at 4 °C. Sections were incubated with secondary antibodies of the same species labeled with HRP primary antibodies for 50 min, and washed with PBS and dropped with freshly prepared DAB chromogenic solution, and the color development time was controlled under a microscope. The positive was brownish-yellow, and the sections were washed with tap water to terminate the color development, and the nuclei were counterstained with hematoxylin for 3 min and dehydrated and mounted. Pictures were collected for quantitative analysis of positive staining. Details of antibodies are provided in Supplementary

Table 2
Sequences of oligonucleotide primers for QRT-PCR.

Gene	Accession numbers	Primer (5′-3′)	Amplicon sizes
β-actin	NM_007393.5	CTACCTCATGAAGATCCTGACC CACAGCTTCTCTTTGATGTCAC	90
Nrf2	NM_010902.4	CAGCCATGACTGATTTAAGCAG CAGCTGCTTGTTTTCGGTATTA	107
Keap-1	NM_001110306.1	GACTGGGTCAAATACGACTGC GAATATCTGCACCAGGTAGTCC	165
HO-1	NM_010442.2	TCCTTGTACCATATCTACACGG GAGACGCTTTACATAGTGCTGT	198
NQO1	NM_008706.5	GAAGACATCATTCAACTACGCC GAGATGACTCGGAAGGATACTG	179
Caspase-3	NM_001284409.1	GAAACTCTTCATCATTCAGGCC GCGAGTGAGAATGTGCATAAAT	250
Caspase-9	NM_001277932.1	TGTGAATATCTTCAACGGGAGC GAGTAGGACACAAGGATGTCAC	249
BAX	NM_007527.3	TTGCCCTCTTCTACTTTGCTAG CCATGATGGTTCTGATCAGCTC	81
Bcl-2	NM_009741.5	GATGACTTCTCTCGTCGCTAC GAACTCAAAGAAGGCCACAATC	156
TNF-α	NM_001278601.1	ATGTCTCAGCCTCTTCTCATTC GCTTGTCACTCGAATTTTGAGA	179
IL-1β	NM_008361.4	CACTACAGGCTCCGAGATGAACAAC TGTCGTTGCTTGGTTCTCCTTGTAC	145
IL-6	NM_001314054.1	CTCCCAACAGACCTGTCTATAC CCATTGCACAACTCTTTTCTCA	97
NF-κB	NM_008689.2	CAAAGACAAAGAGGAAGTGCAA GATGGAATGTAATCCCACCGTA	203

Table 1. The detailed methods were referred to the Supplementary 1.4.

2.5. Detection of inflammatory factors and markers of kidney injury by ELISA

The levels of murine IL-12, IL-6, and IL-10 in mouse serum and cytokine levels of neutrophil gelatinase-associated lipocalin (NGAL) and Kidney Injury Molecule 1 (KIM-1) in mouse serum were determined by ELISA kits (Chenglin Biological, Beijing, China), according to the manufacturer's instructions.

2.6. Western-blot analysis

Renal tissue total protein and cellular total protein were extracted according to the previous method [35]. Nuclear proteins were extracted with a nuclear protein extraction kit. Immunoblotting was performed using antibodies from different companies: Nrf2 (1:1000), Keap-1 (1:1000), HO-1 (1:1000), and NQO1 (1:1000) (Beijing Biosynthesis Biotechnology Technology, Beijing, China); BAX (1:1000), Bcl-2 (1:1000), Caspase-3 (1:1000), Caspase-9 (1:1000) (ABclonal Co, Ltd., Wuhan, China); NF-kB (1:1000), TNF-α (1:1000) (Wanleibio, Harbin, China), and visualized using chemiluminescence agent ECL [36]. Image acquisition was performed using a celestial gel imaging system. Image analysis was performed using ImageJ software for densitometric analysis, and relative protein expression = target protein gray value/β-actin gray value. Details of antibodies are provided in Supplementary Table 1. The detailed methods were referred to the Supplementary 1.2.

2.7. Real-time PCR analysis

Fifty mg of kidney tissue was weighed and ground in a homogenizer containing 1 mL Trizol. Total RNA was extracted and cDNA was synthesized by reverse transcription using HiScript II Reverse Transcriptase (Glycerol-free) kit (Vazyme, Nanjing, China). RT-PCR primers were designed according to the NCBI rat mRNA sequence database (Table 2). After primer synthesis (Shanghai Sangon Biological Co., Ltd, Shanghai, China), the RT-PCR reaction system was prepared according to the requirements of 2 × SYBR Green qPCR Master Mix kit. The relative levels of mRNA were calculated according to the $2_{\triangle\triangle}$Ct method, and β-actin could be used as an endogenous control for normalization. The detailed methods were referred to the Supplementary 1.1.

2.8. NRK52E cytotoxicity assay and In vitro intervention assay

Logarithmic renal tubular epithelial cells (NRK52E cell line was derived from Shanghai Cell Bank, Chinese Academy of Sciences) were cultured as described previously [37]. Cytotoxicity was detected using a CCK-8 assay kit (BS350B, Biosharp, Hefei, China). Cells were plated in 96-well plates at a density of 8000 cells/well. After incubation with AAI (0, 5, 10, 20, 30, 35, 40, 80 μM) and LYC (0, 2.5, 5, 10, 20, 40 μM) for 24 h, 10% CCK-8 solution diluted in serum-free DMEM was added to each well and incubated at 37 °C for 2 h. The absorbance at 450 nm was measured by a microplate reader (Biotek, MQX200, Winooski, VT, USA) [38]. The optimal dosing concentrations of AAI and LYC were selected for subsequent experiments. The experiment was divided into five groups: control group(Con), model group (AAI 40 μM)(AAI), LYC control group (LYC 10 μM)(LYC), LYC high and low dose treatment groups (LYC 5 μM and 10 μM)(AL5 AL10), cells were treated with AAI (40 μM) and pretreated with Nrf2 inhibitor ML385 (5 μM) and Nrf2 activator AKBA (40 μM) [39,40], respectively, and the relevant parameters were measured after 24 h.

Cell viability (%) = ODsample – ODblank/ ODcontrol - ODblank × 100%

2.9. Immunofluorescence detection of Nrf2/NF-Kb/IL-1β

NRK52E cells were plated in 24-well plates and treated with AAI (40 μM) and LYC (10 μM) for 24 h when the density reached 60%–70%. The cells were fixed with 4% paraformaldehyde, washed, permeabilized, and blocked. Cells were incubated with primary antibodies: Nrf2 (1:200), NF-kB (1:200), IL-1β (1:200) overnight at 4 °C in a refrigerator. Secondary antibody Goat Anti-Rabbit IgG HampL/HRP (1:200) was added to the cells for 1.5 h followed by DAPI staining of the nucleus for 2 min. After mounting with PBS, cell plates were placed on an inverted fluorescence microscope, and fluorescence signals were acquired and quantified using Image-Pro Plus software (version 3.0, Media Cybernetics, Bethesda, MD, USA) by using the same parameters [41]. Details of antibodies are provided in Supplementary Table 1. The detailed methods were referred to the Supplementary 1.3.

2.10. Detection of cell morphological structure

NRK52E cells were plated in 24-well plates (1×10^5 cells/well) and treated with AAI (40 μM) and LYC (10 μM) for 24 h when the density reached 60%–70%. Cell plates were photographed under a light electron microscope to evaluate changes in cell morphology. The digested cells were centrifuged at low speed and fixed with 2.5% glutaraldehyde buffered fixative and 1% osmic acid fixative, respectively, and the ethanol in the sample was replaced with acetone after gradient dehydration of the sample with graded ethanol. The cells were then infiltrated into the epoxy resin and embedded. Ultrathin sections of 50 nm–60 nm were prepared. The organelles were observed under a transmission electron microscope.

2.11. Determination of ROS content in cells

NRK52E intracellular ROS was measured with a DCFH-DA fluorescent probe (Nanjing jiancheng Bioengineering Institude, Nanjing, China). The drug-incubated cells were incubated with DCFH-DA (10 μM) for 30 min in a humidified chamber in the dark. Fluorescence signals were acquired and quantified using Image-Pro Plus software (version 3.0, Media Cybernetics, Bethesda, MD, USA) by using the same parameters.

2.12. Detection of apoptosis

After the cell density reached 60%–70%, the cells were treated with AAI (40 μM) and LYC (10 μM) for 24 h. After 24 h, (1×10^5 - 5×10^5) cells were collected and treated according to the requirements of Annexin V-FITC/PI Apoptosis Detection Kit (A005-1-3, Bioss, Beijing, China), and then analyzed using flow cytometry. Annexin +/PI − cells were identified as early apoptotic cells, and Annexin +/PI + cells were identified as late apoptotic cells [8].

2.13. Morphology of nuclei detected by DAPI staining

Cells (2×10^5 cells/well) were seeded into 24-well plates. After treatment with AAI concentrations (10, 20, and 40 μM) and LYC (5 and 10 μM) for 24 h. After washing the cells with cold PBS, the cells were fixed in 4% paraformaldehyde for 10 min at room temperature. DAPI staining solution (10 μg/mL, 200 μL/well) (Biosharp, Hefei, China) was added for 10 min in the dark. The cell plate was placed on an inverted fluorescence microscope to observe the morphological changes of the nucleus (excitation wavelength of 352 nm) [39].

2.14. Statistical analysis

All experimental data were analyzed using ImageJ, Graph-Pad Prism 8.0.2 and SPSS 22.0. Repeated independent tests were taken. Data are presented as mean ± SEM. Data were analyzed using the one-way

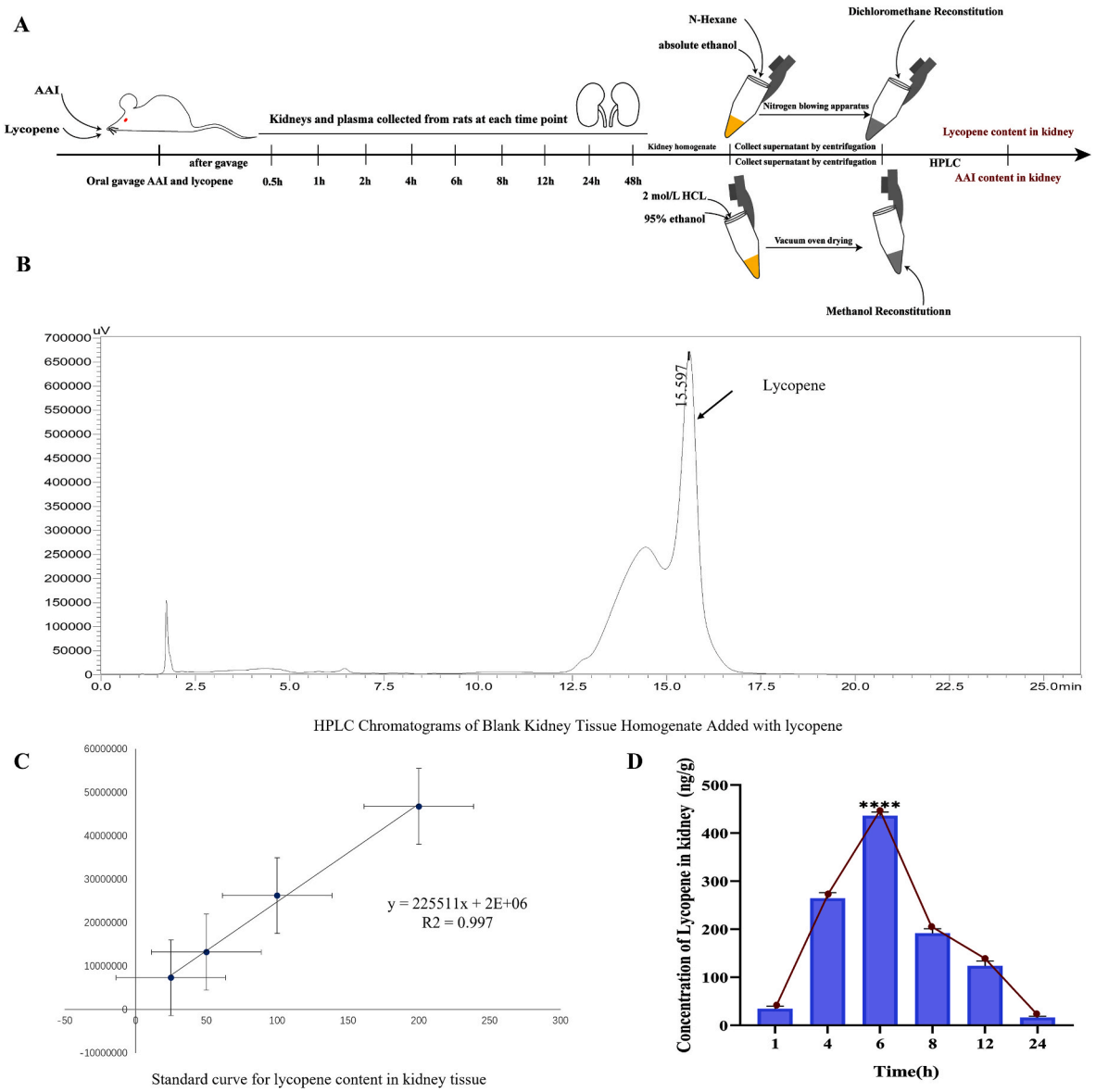

Fig. 1. Lycopene content in kidney at different time points. A: Experimental flowchart for detecting AAI and lycopene contents in rat kidney following oral gavage administration of AAI and lycopene. B: HPLC chromatograms of blank kidney tissue homogenate added with lycopene. The lycopene standard showed a peak at approximately 15 min. C: Content of lycopene in kidney at different time points after intragastric administration of lycopene.

variance method. Differences among groups of data were tested using the least significant difference and Duncan's multiple comparison method. $P < 0.05$ was considered statistically significant. Principal component analysis (PCA) and Pearson correlation (PCC) were performed using Origin 2021.

3. Results

3.1. Detection of lycopene in rat kidney after oral administration of lycopene

In order to verify the metabolism of AAI and lycopene in the kidney, we examined the contents of the two drugs in the renal tissue of rats at various time points after administration of AAI and lycopene. The specific experimental flow is shown in Fig. 1-A. First, we verified whether lycopene can be metabolized to the kidney within 24 h after oral gavage of lycopene. The results of HPLC showed that the peak time of lycopene standard was about 15 min when lycopene standard was added to the kidney homogenate of blank rats. And the measured peak area showed a linear relationship with the concentration of lycopene standard, (R2 > 0.99) (Fig. 1-B, C). However, when the content of lycopene in the kidney tissue of blank rats was detected alone, no peak was observed at about 15 min. Therefore, the results showed that compared with blank rats, the content of lycopene in the kidney of rats in the lycopene gavage group was the highest after oral gavage for 6 h. The lycopene content in the kidney gradually decreased after 6 h and the content was almost 0 after 24 h (Fig. 1-D, Supplementary Figs. 3–A ~ H).

3.2. Effect of lycopene on AAI content in rat kidney

The peak appearance time of AAI standards was approximately 7.5 min each (Fig. 2-C). And the concentration of AAI standard was in the range of 2.5–20 μg/ml. The peak areas of samples were positively correlated with concentrations and showed a good linear relationship (R2 > 0.99). And the precision, stability, and recovery of AAI standards in kidney met the requirements. In this study, AAI was detected in rat kidney at 0.5 h and 2 h after oral gavage of AAI. And at 0.5 h, AAI was more abundant in the kidney. AAI was not detected at other time points.

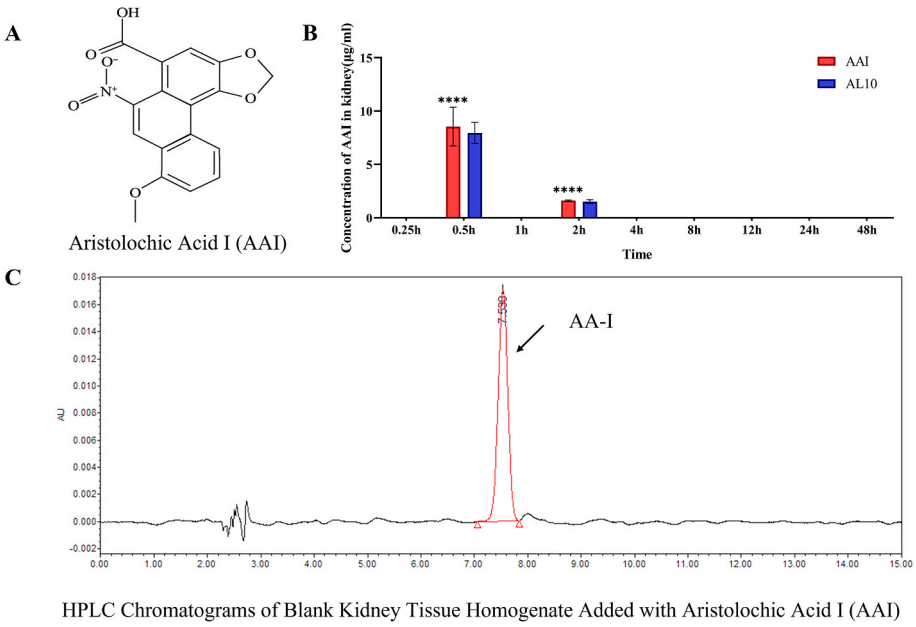

HPLC Chromatograms of Blank Kidney Tissue Homogenate Added with Aristolochic Acid I (AAI)

Fig. 2. Aristolochic acid content in kidney at different time points. A: Chemical Formula of Aristolochic Acid. B: Changes of AAI content in kidney at different time points after intragastric administration of AAI. C: HPLC Chromatograms of Blank Kidney Tissue Homogenate Added with AAI. The AAI standard showed a peak at approximately 7.5 min.

Table 3
Changes of AA-I contents in kidney of rats.

Time	Group AAI	Group AAI + LYC
15min	0	0
30min	8.546161319 ± 1.478004697	7.955484348 ± 0.810681218
1h	0	0
2h	1.61552925 ± 0.047434393	1.51552925 ± 0.149291833
4h	0	0
8h	0	0
12h	0	0
24h	0	0
48h	0	0

These results indicate that AAI has been metabolized completely in the kidney 2 h after feeding. Furthermore, no accumulation of ALI, a metabolite of AAI in the kidney, was demonstrated after 2 h (Figs. S2–B). And there was no significant difference in the content of AAI in the kidney of rats fed with lycopene compared with rats fed with AAI alone (Fig. 2-B, Table 3).

3.3. Lycopene attenuates aristolochic acid-induced renal histopathological changes

From the clinical manifestations and pathological anatomy results, it can be seen that mice in the AAN group showed typical features of aristolochic acid nephropathy: rough hair, small body size, and significantly reduced body weight. Necropsy of mice in the AAN group showed the kidneys were whitish in color and smaller in size. Compared with the control group, the renal index of mice in the AAN group was significantly lower. However, mice in the AL20 group had increased body weight and decreased renal index. These results indicated that lycopene intervention significantly ameliorated AAN in mice (Fig. 3-B, C, D). Pathological examination with HE and PAS staining showed that the renal tubular structure of mices in the normal group and LYC group were intact without signs of lesions. In the AAN group, the pathological phenomena of tubular dilatation, disappearance of brush border, formation, tubular epithelial cell detachment, karyolysis, inflammatory cell infiltration, and glomerular atrophy occurred. The scores of renal histopathology and tubular injury were significantly increased in mice in the AAN group. Interestingly, there was a significant improvement in damaged renal tissue in mice with AAN after lycopene intervention. (Fig. 3-E, F, G).

3.4. Lycopene ameliorated renal dysfunction and oxidative stress injury in AAN mice

Renal function tests showed that Cr and BUN levels in the serum of mice in the AAN group were significantly higher than those in the control group. While Cr and BUN levels in the serum of mice in the LYC group were significantly lower (Fig. 4-A, B). Kidney injury factor-1 (KIM-1) and neutrophil gelatinase-associated apolipoprotein (NGAL) are markers of tubular injury [42,43]. The results showed that lycopene significantly reduced the expression levels of KIM-1 and NGAL induced by AAI (Fig. 4-C, D). In addition, the results showed that lycopene significantly decreased the expression of AAI-induced lipid peroxidation product (MDA), and increased the expression of antioxidant enzyme systems (T-AOC, SOD, and GSH-PX) (Fig. 4-E, F, G, H). These results indicate that lycopene is able to alleviate renal dysfunction and renal oxidative stress damage in AAN mice.

3.5. Lycopene improves inflammatory responses in the kidneys of AAN mice

It is known that the expression of inflammatory factors in the kidney is increased when the kidney have an inflammatory response. And renal interstitial fibrosis occurs in chronic kidney disease due to the continuous occurrence of inflammatory reactions. In this experiment, the results of MASSON staining showed that the renal interstitium of mice in the AAN group was severely fibrotic compared with the control group. Degree of renal fibrosis was alleviated after LYC intervention (Fig. 5-A, B). Our results by Western-blot, RT-PCR and ELISA revealed that the expression of TNF-α, IL-6, IL-10, was increased and the expression of IL-12 was decreased in the kidneys of model mice compared with the control group. However, LYC intervention reversed the expression of these genes in a dose-dependent manner, (Fig. 5-D, E, F, G, H). These results illustrate that LYC is able to ameliorate the inflammatory response caused by AAI, which in turn alleviates the development of

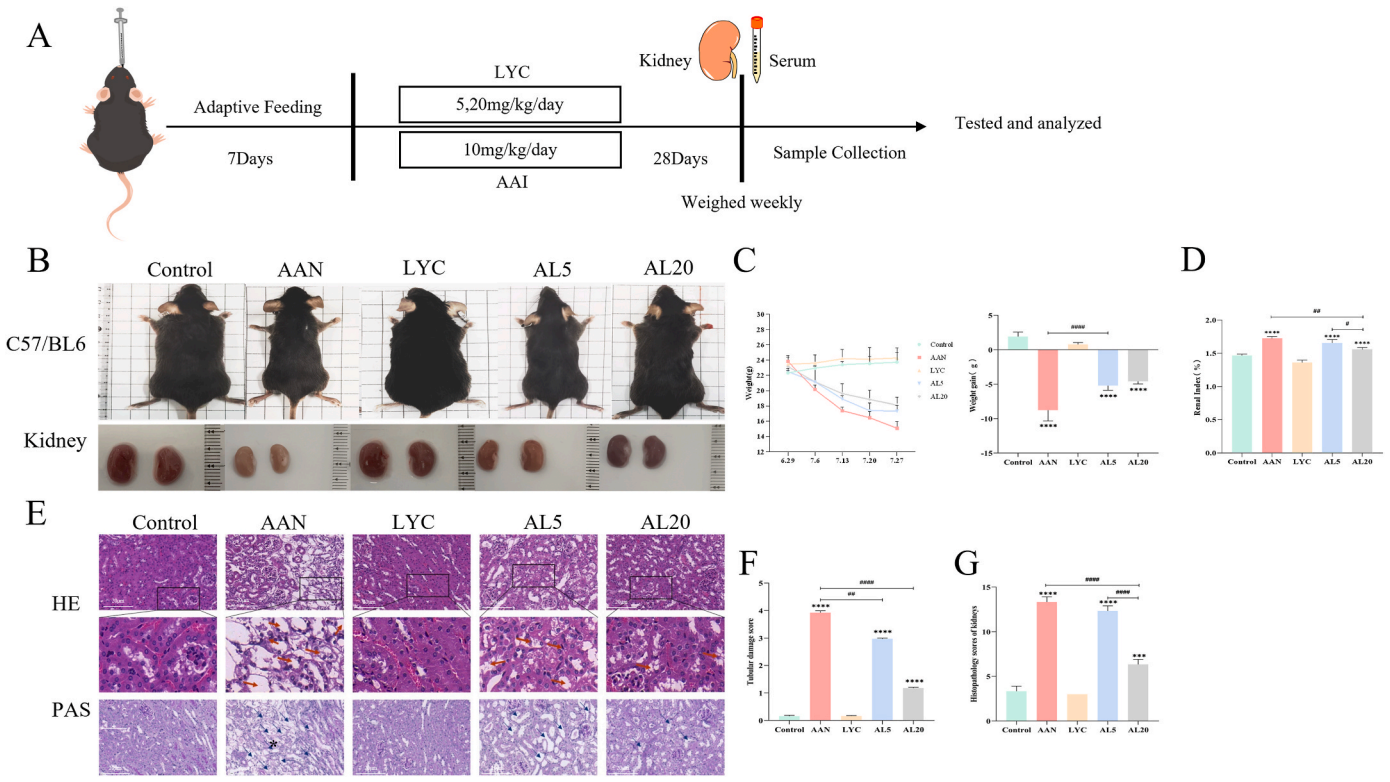

Fig. 3. Clinical and histopathological effects of LYC on aristolochic acid nephropathy (AAN). A: Schematic diagram of establishment of animal model. B: Photograph of the mouse after the last treatment, and photograph of the kidney after sample collection. C–D: body weight and kidney coefficient of mice. E: HE staining (200 × and 400 ×) and PAS staining (200 ×) of mouse renal tissues. F: Plot of tubular injury scores. G: Histopathological score of kidney. (In HE staining diagram, yellow arrow indicated inflammatory cell infiltration, renal tubular vacuole and epithelial cell detachment); (In PAS staining diagram, blue arrow indicated renal tubular injury and asterisk indicated the formation). Compared with the control group, * indicates $p < 0.05$, ** indicates $p < 0.01$, *** indicates $p < 0.001$, and **** indicates $p < 0.0001$; Comparison between Other Groups, $^{\#}$ indicates $p < 0.05$, $^{\#\#}$ indicates $p < 0.01$, $^{\#\#\#}$ indicates $p < 0.001$, and $^{\#\#\#\#}$ indicates $p < 0.0001$. (For interpretation of the references to color in this figure legend, the reader is referred to the Web version of this article.)

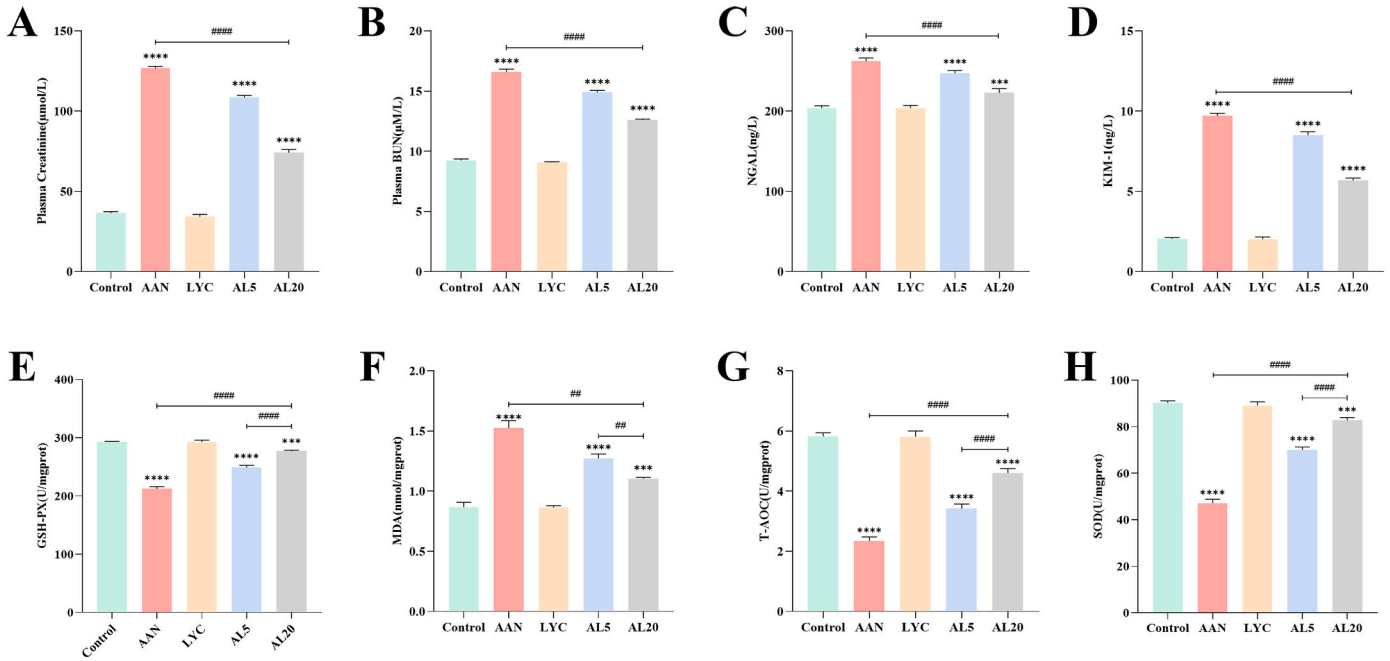

Fig. 4. Effects of LYC on renal function and oxidative stress in AAN mice. A: The content of creatinine in the serum of mouse. B: Content of urea nitrogen in mouse serum. C–D: The content of renal injury factor KIM-1 and neutrophil gelatinase-associated lipocalin NGAL in mouse serum. E–H: The contents of oxidative stress markers MDA, GSH-PX, SOD, and T-AOC in the serum of mice.

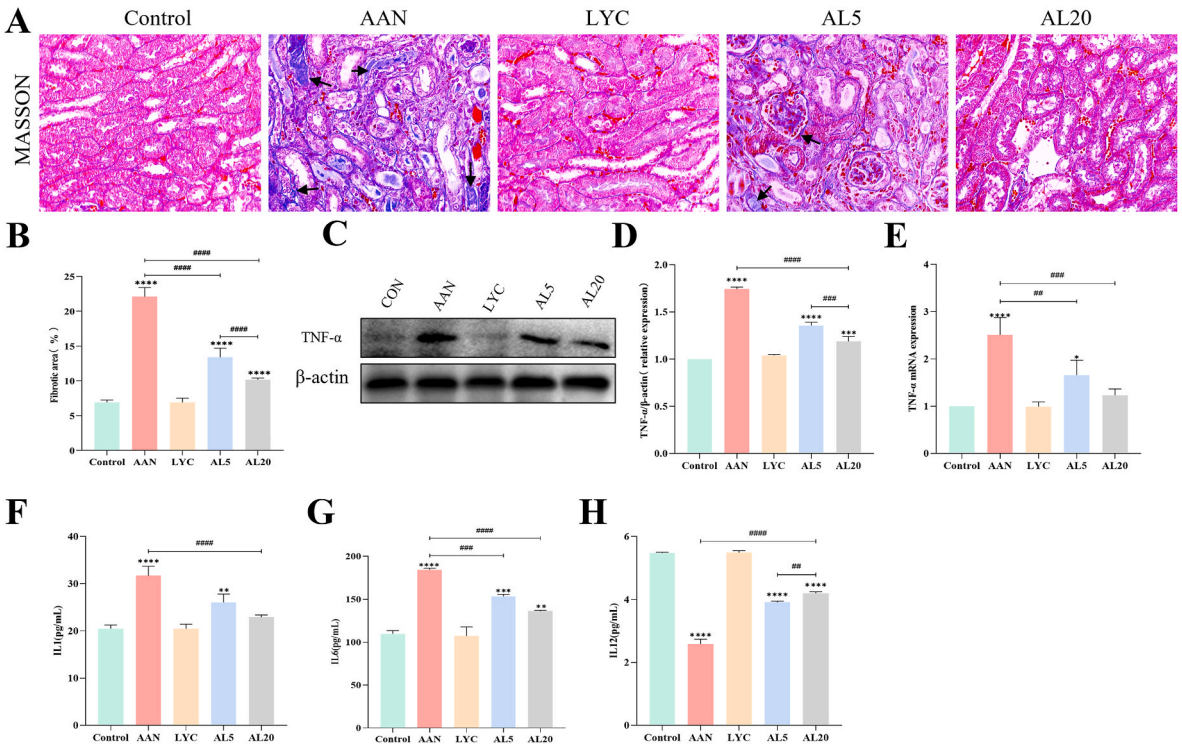

Fig. 5. LYC alleviated renal fibrosis as well as high expression of inflammatory factors and tumor necrosis factor-α in the kidney of AAN mice. A: Representative images of MASSON staining in each group. B: Percentage of fibrosis-positive area in kidney sections. C-E: Western-blot and RT-PCR detected the expression of TNF-α. ($x \pm s$, $n \geq 3$). F–H: The contents of IL-1, IL-6 and IL-12 in kidney were detected by ELISA.

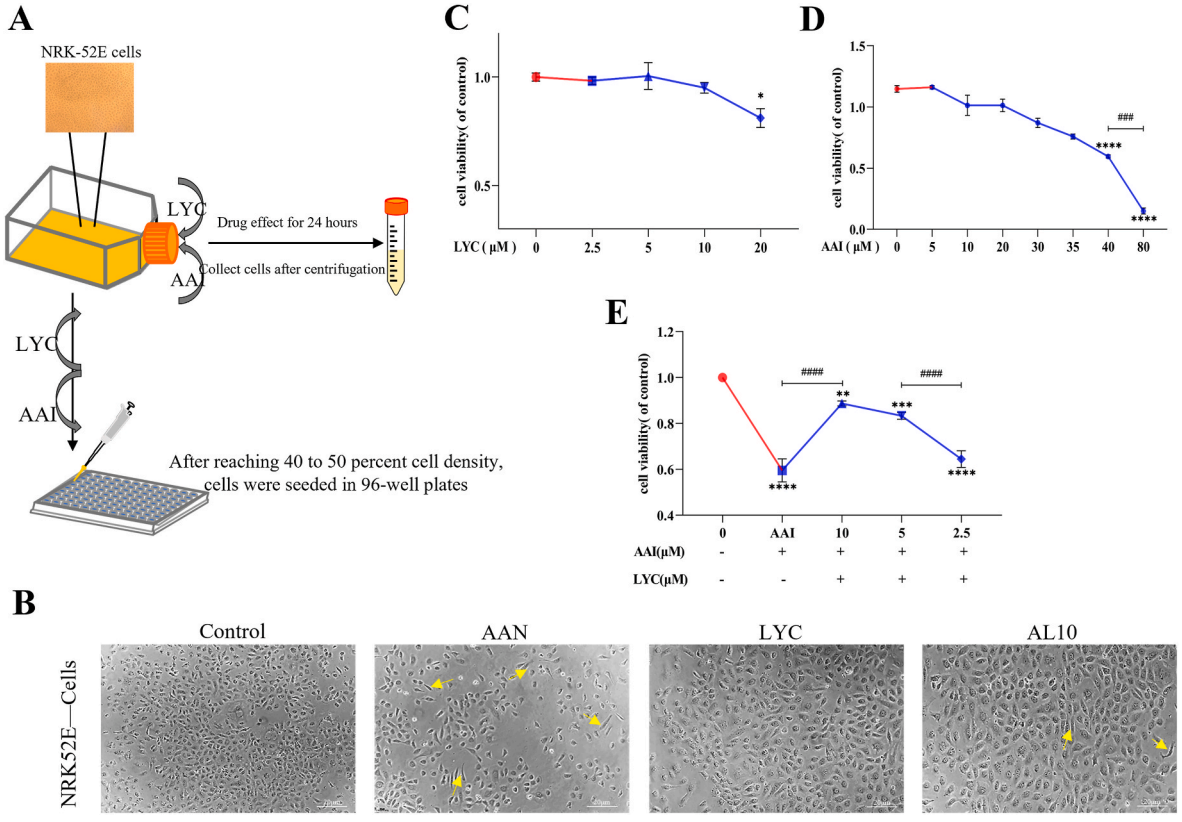

Fig. 6. Effects of LYC on viability and virulence of NRK52E cells exposed to AAI. A: Flow chart of cell experiments. B: Cell morphology and growth rate were observed under a light microscope. C: Effect of AAI at different concentration gradients on NRK52E cell viability. D: Effect of LYC at different concentration gradients on NRK52E cell viability. E: CCK8 assay was used to detect the effect of AAI and lycopene on the viability of NRK52E cells.

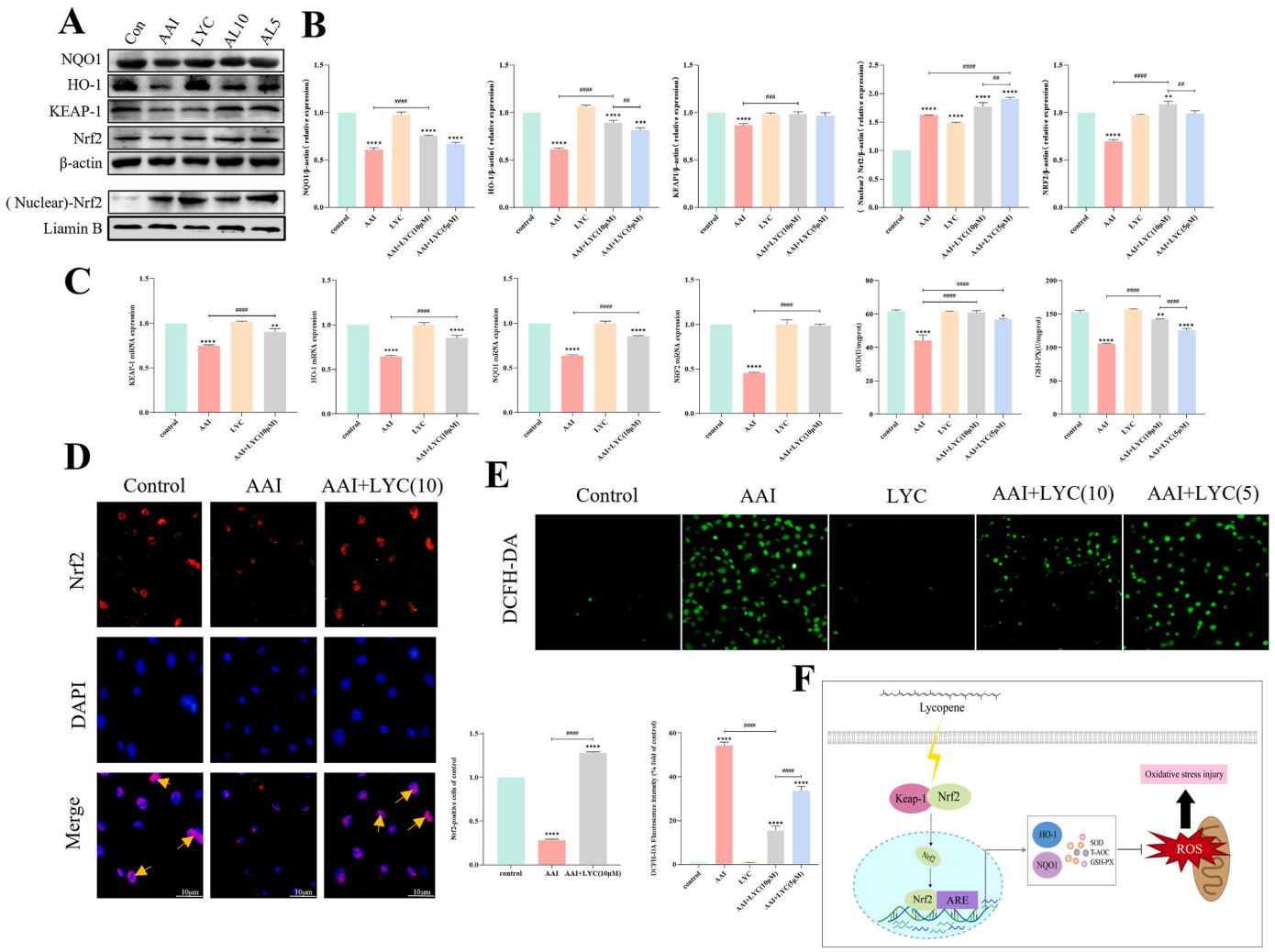

Fig. 7. LYC promoted Nrf2 nuclear translocation and activated downstream antioxidant signaling pathways to alleviate AAI-induced oxidative stress injury in NRK52E cells. A–C: Western-blot and RT-PCR detected the expression of HO-1, NQO1, Keap-1, Nuclear-Nrf2, and Nrf2. Elisa detected the intracellular SOD and GSH-PX expression. D: Immunofluorescence detected the expression of Nrf2 in the cells and the positive expression areas were quantified. "Yellow arrows" in the figure indicated the phenomenon of Nrf2 nuclear translocation. E: In vitro DCFH-DA staining was performed on NRK52E cells after drug treatment to detect the content of intracellular ROS and quantitative analysis of fluorescence intensity. F: Schematic representation of Nrf2 signaling pathway mechanism. (For interpretation of the references to color in this figure legend, the reader is referred to the Web version of this article.)

AAI-induced chronic kidney disease.

3.6. *Lycopene attenuates AAI-induced toxicity in NRK52E cells*

The drug intervention process in cell experiments is shown in Fig. 6-A. When the cell density reached 40%–50%, the drug was added to the cell culture medium by changing the solution. In order to investigate the toxic effect of AAI on cells and the optimal concentration of AAI and LYC, we used light microscopy to observe the morphology of cells in each group after administration. In the control group, the cell morphology was round or oval and the degree of cell fusion reached more than 90%. The morphology of cells in the AAI group was altered. Some cells showed a long shuttle shape and were in a poor state. The degree of cell fusion was about 50% and the growth rate was slow. while after LYC intervention, the cell state was improved. The long shuttle cells were reduced, and the cell fusion degree reached about 80% (Fig. 6-B). When the concentration of AAI was 40 μM, the viability of the cells was 60%. This was the optimal concentration required for the experiment (Fig. 6-C, D). When the cells were treated with LYC (5 μM, 10 μM) together with AAI for 24 h, the cell viability was reduced in the AAI group. Cell viability increased after LYC treatment in a dose-dependent manner (Fig. 6-E).

3.7. *Lycopene activates Nrf2-HO-1 antioxidant pathway to inhibit oxidative stress injury induced by AAI exposure in NRK52E cells*

The results of Western-blot, RT-PCR, and ELISA showed that the expression of Nrf2, Keap-1, HO-1, NQO1, GSH-PX, and SOD in NRK52E cells decreased after AAI exposure compared with the control group, and the expression in the Nrf2 nucleus increased. After LYC intervention, these were reversed: as shown by a significant increase in Nrf2 intranuclear expression and a significant decrease in the content of ROS in a dose-dependent manner (Fig. 7-A, B, C, E). Immunofluorescence staining of AAI and LYC treated cells was performed using Nrf2 antibody. The results showed that LYC intervention could significantly increase the expression of Nrf2 in the nucleus (Fig. 7-D). These results suggest that LYC inhibits AAI-induced oxidative stress and the overexpression of ROS by activating the antioxidant system of Nrf2/Keap-1, ultimately reducing oxidative damage in the body. According to the results of this experiment, the mechanism of Nrf2 signaling pathway was plotted (Fig. 7-F).

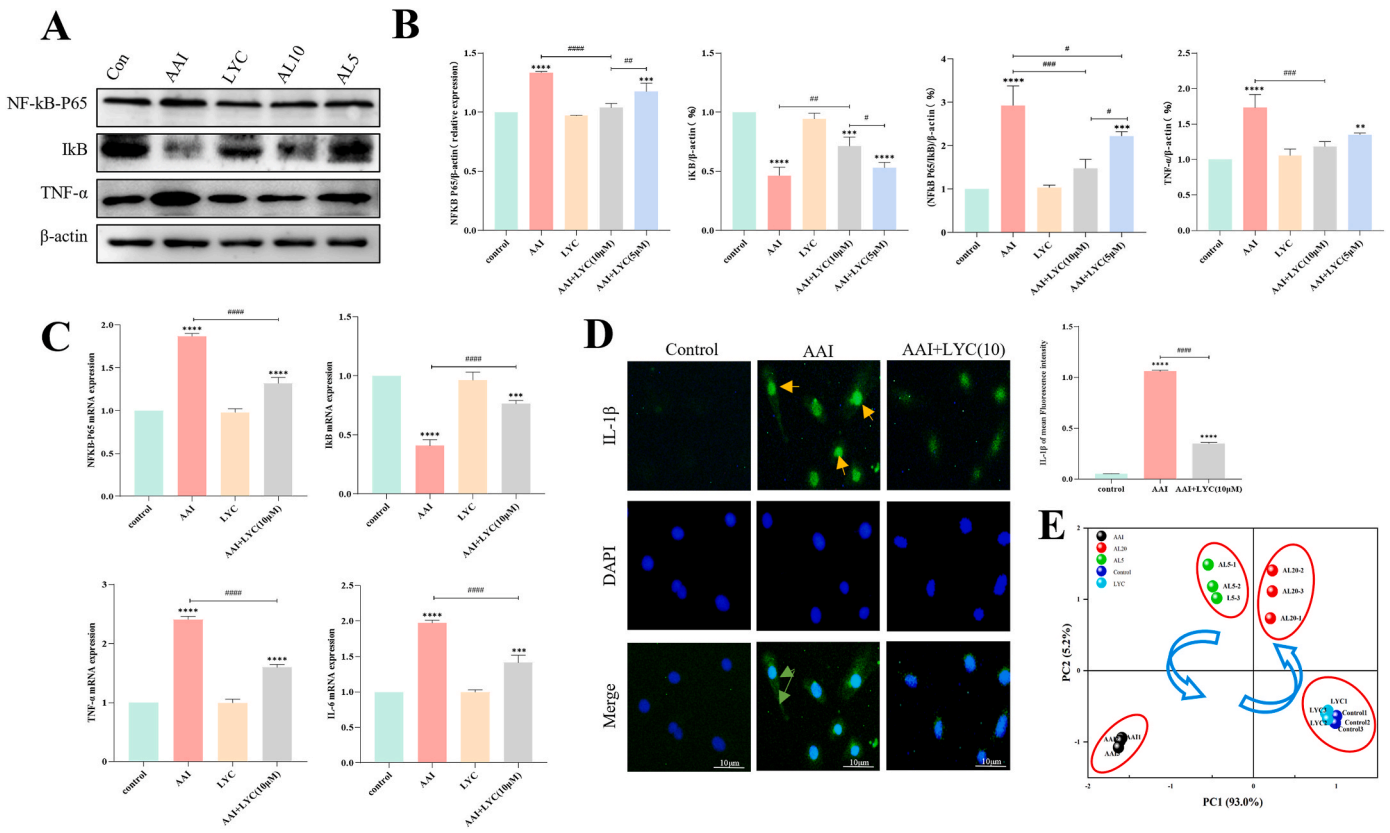

Fig. 8. LYC inhibited the TNF-α, NF-κB signaling pathway to reduce the release of inflammatory factors and attenuated AAI-induced inflammatory injury in NRK52E cells. A–C: Western-blot and RT-PCR detected the expression of TNF-α, NF-κB-p65, IkB, and IL-6. D: Immunofluorescence detected the expression of IL-1β in NRK52E cells and the positive expression areas were quantified. E: PCA score plot of Nrf2 and NF-κB system-related parameters.

3.8. Lycopene regulates TNF-α/NF-κB signaling pathway to inhibit AA-I-induced inflammatory response in NRK52E cells

To explore the effects of LYC and AAI on the NF-κB signaling pathway, we examined the levels of NF-κB and its downstream target genes in the kidney. The results of Western-blot, RT-PCR and immunohistochemistry showed that the expression of NF-κB-p65, TNF-α, and IL-6 was increased and the expression of IkB and IL-12 was decreased in the cells of the AAI group compared with the control group. LYC treatment reversed the expression of these proteins (Fig. 8-A, B, C).Immunofluorescence staining of AAI and LYC treated cells was performed using IL-1β antibody. The results showed that LYC treatment significantly decreased the expression of IL-1β in the cells compared with the AAI group (Fig. 8-D).These results indicated that LYC can inhibit TNF-α and NF-κB signaling pathways and then inhibit AAI-induced inflammatory responses.In addition, PCA was used to detect the parameters of Nrf2 system and NF-κB signaling pathway target genes (Fig. 8-E).The results showed that PC1 and PC2 were 93% and 5.2%, respectively. The counterclockwise direction from Control group to AAI group indicated a dose-dependent manner. The close location of Control group and AL20 group in the figure indicated that LYC can alleviate AAI-induced oxidative stress and inflammation in NRK52E cells by activating the Nrf2 system and inhibiting the NF-κB signaling pathway. These results illustrated that LYC is able to inhibit the inflammatory response caused by AAI and attenuate the damage of AAI to renal tubules by acting on the NF-κB signaling pathway.

3.9. Lycopene inhibits AAI-induced mitochondria-dependent apoptosis

Mitochondrial damage is a major factor in apoptosis. In order to explore the effect of LYC and AAI on apoptosis, we observed the cells in each group using transmission electron microscopy and detected the expression levels of apoptosis-related genes in the cells. Transmission electron microscopy showed that there were no abnormal findings in the nucleus, cytoplasm, mitochondria and other organelles in the control group. While nuclear pyknosis, as well as swelling, vacuolization, fragmentation of a large number of mitochondria, breakage and disappearance of mitochondrial ridges, and the presence of apoptotic bodies were observed in the AAI-exposed cells, (marked with arrows in the figure). After LYC intervention, cellular mitochondrial damage was significantly reduced, (Fig. 9-A). Western-blot and RT-PCR results showed that the expression of Bax, Cleaved-Caspase3, and Cleaved-Caspase9 was increased and the expression of Bcl-2, Caspase-3, and Caspase-9 was decreased in the cells of the AAI group compared with the control group. However, LYC reversed the expression of these proteins after intervention (Fig. 9-B, C, D). The results of the number of apoptotic cells determined by flow cytometry showed that the number of apoptotic cells (early and late) was significantly increased in the AAI group compared with the control group. The number of apoptotic cells was significantly decreased after LYC intervention (Fig. 9-E). These data suggest that AAI caused cell damage, with apoptosis being the major pathway. LYC, on the other hand, was able to alleviate the occurrence of apoptosis.

3.10. Activation of Nrf2 nuclear translocation is key to LYC inhibition of NRK52E cells oxidative stress

To further verify whether Nrf2 acts as a target for LYC to attenuate AAI-induced oxidative stress. We added inhibitors and activators of Nrf2 nuclear translocation to cells in vitro and performed a series of experiments. It was found that the expression of Nrf2, Keap-1, HO-1, NQO1 decreased and the content of ROS increased in the AAI group compared

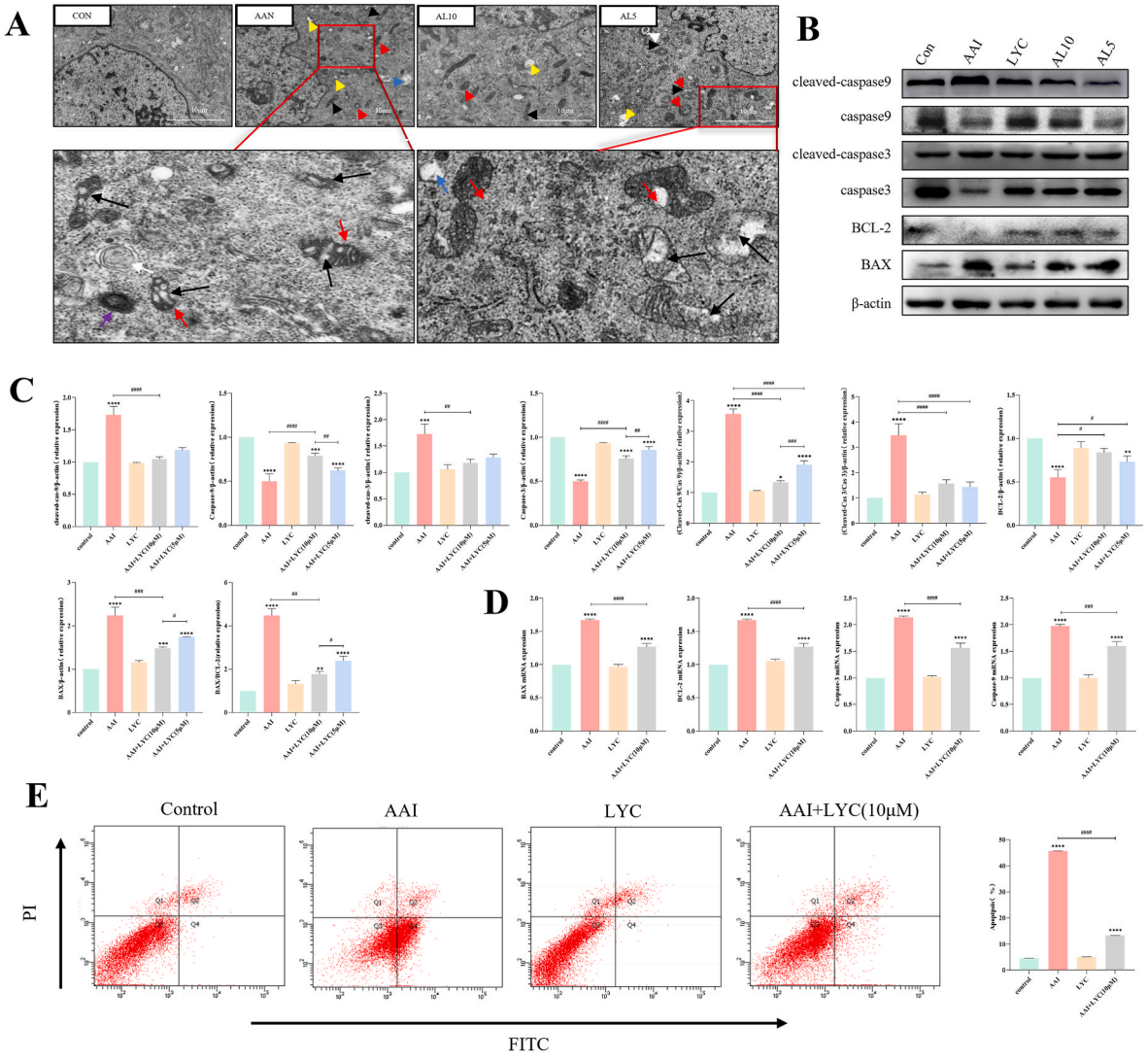

Fig. 9. LYC inhibited mitochondrial damage and regulates apoptotic genes to inhibit AAI-induced apoptosis in NRK52E cells. A: Transmission electron microscopy of NRK52E cells. "Red arrow" indicated mitochondrial swelling; "Black arrow" indicated mitochondrial membrane dissolution, mitochondrial cristae disappeared and vacuolized; "Yellow arrow" indicated tubular epithelial cell vacuolization; "White arrow" indicated autophage; "Purple arrow" indicated apoptotic body; "Blue arrow" indicated residual vacuoles after autophage digestion. B, C: Western-blot detected the expression of BAX, Bcl-2, Caspase-3, Cleaved- Caspase-3, Caspase-9 and Cleaved-Caspase-9. D: RT-PCR analyzed the mRNA expression of BAX, Bcl-2, Caspase-3 and Caspase-9. E: Annexin-V-fluorescein isothiocyanate (FITC) and propidium iodide (PI) staining to identify apoptosis by flow cytometry and quantitative summary data of different apoptosis. (For interpretation of the references to color in this figure legend, the reader is referred to the Web version of this article.)

with the control group. The expression of these genes was elevated and the content of ROS decreased after LYC intervention. However, when the Nrf2 inhibitor ML385 was added, the effect of LYC was significantly reduced or even ineffective (Fig. 10-A, B, and D). In contrast, when the Nrf2 activator AKBA was added, it increased the expression of Nrf2, keap-1, HO-1, NQO1 and decreased the content of ROS in the cells (Fig. 10-E, F). The trend of action between Nrf2 activators and LYC was consistent. The cell viability assay results showed that ML385 reduced cell viability to approximately 50%. However, the viability of cells co-treated with AKBA and AAI increased to 80%, (Fig. 10-C, G). In summary, these data demonstrated that nuclear translocation of Nrf2 is a target for LYC to attenuate AAI-induced oxidative stress.

3.11. Inhibition of oxidative stress is a prerequisite for lycopene to inhibit apoptosis and inflammatory responses

LYC increased Nrf2 nuclear translocation and further verified whether inhibition of Nrf2 nuclear translocation would block the inhibitory effect of LYC on NF-κB signaling pathway and apoptosis. The results showed that the expression of NF-κB, TNF-α, Bax, and Cleaved-Caspase-3 was increased and BCL-2 expression was decreased in the AAI group compared with the control group. LYC significantly reversed the expression of these genes. However, when the Nrf2 inhibitor ML385 was added, the effect of LYC was significantly reduced or even ineffective (Fig. 11-A, B). In contrast, when the Nrf2 activator AKBA was added, it similarly decreased the expression of NF-κB, TNF-α, Bax, Cleaved-Caspase3, and increased the expression of Bcl-2 (Fig. 11-D, E). Immunofluorescence staining of AAI, LYC and ML385-treated cells was performed using NF-κB-P65. NF-κB-P65 nuclear expression was significantly increased in the AAI group. But NF-κB-P65 nuclear expression was significantly decreased after LYC intervention. The addition of ML385 inhibited the effect of LYC. The increased expression of NF-kB-p65 in the nucleus was more pronounced after treatment with AAI and ML385 (Fig. 11-C, G). The results of DAPI staining showed that the nuclei of the control group were regularly oval in shape. Most of the cells had uniform and morphologically intact nuclear staining as well as

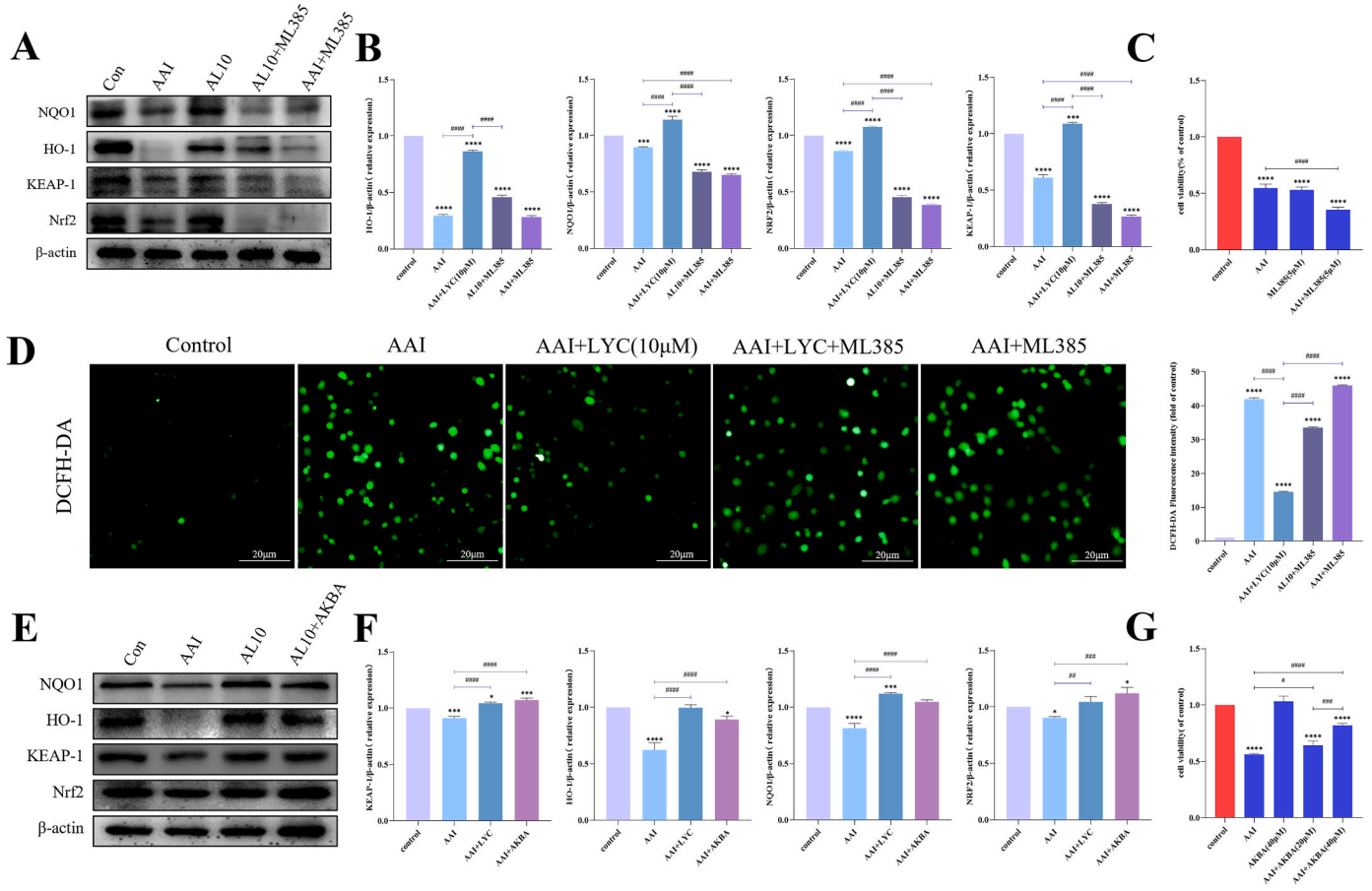

Fig. 10. The effect of nuclear translocation of Nrf2 on LYC slowing oxidative stress in NRK52E cells. A, B: Western-blot detected the protein expression of Nrf2, HO-1, NQO1 and Keap-1. C: Cell viability was measured by CCK8 assay. D: The content of intracellular ROS and quantitative analysis of fluorescence intensity. E, F: Western-blot detected the protein expression of Nrf2, HO-1, NQO1, and Keap-1.

uniform dispersion of chromatin throughout the nucleus. Upon addition of AAI, typical apoptotic morphological changes occurred. In the AAI group, nuclear fragmentation, chromosome condensation, chromatin fragmentation, chromosome edge condensation in the periphery of the nuclear membrane, and nuclear shrinkage occurred. LYC intervention could alleviate the AAI-induced changes in nuclear morphology and reduce the number of apoptotic cells. But the effect of LYC was inhibited after the addition of ML385, which could not reverse the occurrence of apoptosis (Fig. 11-F). The above results illustrated that LYC can activate the antioxidant pathway of Nrf2, which in turn inhibits the NF-κB signaling pathway and the development of apoptosis.

3.12. Lycopene activates the Nrf2 antioxidant system to inhibit the development of renal inflammation and apoptosis in AAN mice

The results of in vitro experiments showed that LYC was able to activate downstream antioxidant pathways by promoting Nrf2 nuclear translocation. It further inhibits inflammatory signaling pathways and apoptosis. In order to verify the accuracy of the results, we performed relevant experiments in vivo. The results of Western-blot, RT-PCR, ELISA and immunohistochemical experiments showed that Nrf2, Keap-1, HO-1, NQO1, GSH-PX and SOD expression decreased in the kidneys of mice in the AAN group. However, lycopene treatment reversed the expression of these proteins (Fig. 12-A, B, C, D, E). These results showed that LYC was able to activate the Nrf2 antioxidant system in the kidney and inhibit oxidative stress injury in the kidney of AAN mice. In addition, compared with the control group, the expression of NF-κB-p65 and downstream target genes (TNF-α, IL-6, IL-10, IL-1β) was increased and the expression of IκB and IL-12 was decreased in the kidney of AAN mice. While LYC intervention reversed the expression of these genes in a dose-dependent manner (Fig. 13–A, B, C, D, E). The expression levels of apoptosis-related genes in renal tissues were examined. Results showed that the expression of Bax, Cleaved-Caspase3, and Cleaved-Caspase9 was increased and the expression of Bcl-2, Caspase-3, and Caspase-9 was decreased in the kidneys of mice in the AAN group compared with the control group. On the other hand, LYC reversed the expression of these proteins in a dose-dependent manner (Fig. 14-A, B, C, D). Further combined with the gene heatmap, it can be seen that LYC treatment significantly activated the Nrf2 antioxidant system and inhibited NF-κB inflammatory signaling pathway, as well as apoptosis of mitochondria-dependent pathway in mouse kidney.

3.13. Correlation analysis of Nrf2 system with NF-kB inflammatory signaling pathway and apoptosis

Pearson correlation coefficient (PCC) was used to compare the association between NF-kB-related pathways, key factors of apoptosis, and the Nrf2 system, (Fig. 15). As can be seen, the mRNA expression of Nrf2 and its downstream target genes was negatively correlated with Bax and Caspase-3 and Caspase-9 levels in the kidney. However, it was positively correlated with GSH, SOD, and Bcl-2 activities. The mRNA expression of NF-kB activity in the kidney was negatively correlated with Nrf2, NQO1, HO-1, and BCL-2 levels. However, it was positively correlated with Bax and Caspase-3 and Caspase-9 levels. In conclusion, the results showed that the Nrf2 system was significantly negatively correlated with NF-kB signaling pathway and apoptosis of mitochondria-dependent pathway ($P < 0.01$, $P < 0.001$, $P < 0.0001$).

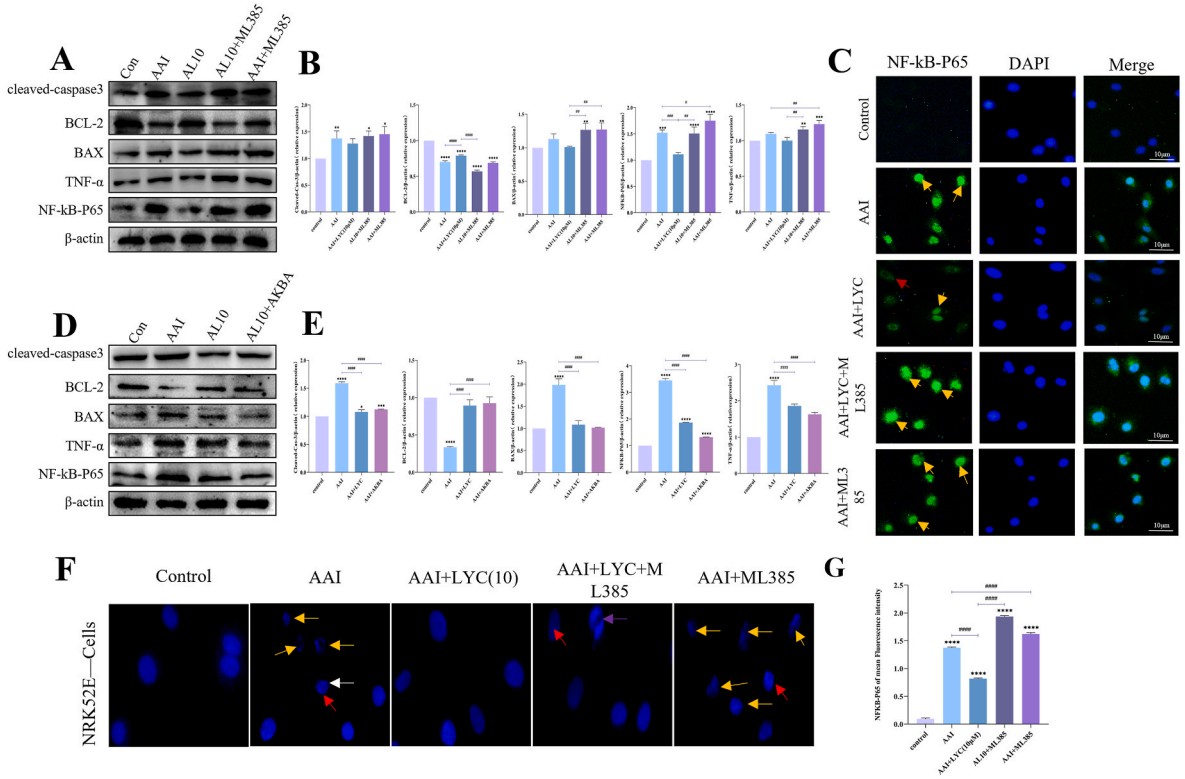

Fig. 11. LYC inhibited the activation of the nuclear translocation NF-κB signaling pathway of Nrf2 and the effects of apoptosis. A–B: Western-blot detected the protein expression of BAX, BCL-2, Cleaved-Caspase3, NF-κB-p65 and TNF-α. C, G: Immunofluorescence detected the expression of NF-κB-p65 in NRK52E cells. "Yellow arrow" indicating positive expression; "Red arrow" indicating extranuclear expression. The positive expression areas were quantified. D–E: Western-blot detected the protein expression of BAX, BCL-2, Cleaved-Caspase3, NF-κB-p65 and TNF-α. F: NRK52E cells were treated with the drug for 24 h. DAPI staining was used to assess nuclear chromatin changes (apoptosis). "Yellow arrow" indicated fragmented nuclei; "White arrow" indicated condensed chromosomes; "Purple arrow" indicated marginalized chromosome condensation; "red arrow" indicated shrunken nuclei. (For interpretation of the references to color in this figure legend, the reader is referred to the Web version of this article.)

4. Discussion

Aristolochic acid nephropathy is an interstitial nephritis caused by AA characterized by a rapid decline in renal function [44]. It is frequently associated with end-stage renal disease and urothelial malignancies [45]. It is characterized by tubular cell apoptosis, necrosis, oxidative stress, inflammatory storm [41], which further leads to renal cell fibrosis [46,47] and ultimately renal failure [48]. At present, there is no effective radical cure. LYC is a natural strong antioxidant from a wide range of sources with antioxidant, anti-inflammatory, and anticancer efficacy. Studies have shown that LYC is able to reduce homocysteine levels and oxidative damage in rat liver [49]. Oral administration of LYC inhibited IL-1β-induced inflammatory injury [22]. As well as LYC was able to inhibit p38-MAPK and JNK inflammation-related pathways showing a maze activity [50]. Previously, it was demonstrated that LYC supplementation attenuates nephrotoxicity caused by ionic disturbances caused by ATR [51]. In this experiment, the pharmacokinetics of lycopene was studied in rats. The results showed that the content of lycopene in kidney was the highest 6 h after oral administration of lycopene. And the content in the kidney gradually decreased after 6 h. It was therefore able to demonstrate that the kidney is one of the target organs of lycopene. Based on the results of the HPLC assay for AAI content in the kidney in this study, the metabolism time of AAI in the kidney was 2 h. And there was no accumulation of AAI and its metabolite ALI in the kidney after 2 h. And this study found that lycopene had no significant effect on the accumulation of aristolochic acid in the kidney when both aristolochic acid and lycopene were intragastrically administered simultaneously. Previous studies have shown that lycopene is most abundant in the kidney 6–8 h after oral gavage of lycopene. Therefore, in order to avoid the effect of co-administration of aristolochic acid and lycopene on renal intake of aristolochic acid, we chose to orally administer AAI at 8:00 a.m. and lycopene at 13:00 p.m. in this experiment. In order to ensure that simultaneous intragastric administration of lycopene will not interfere with the establishment of aristolochic acid nephropathy model. It was further demonstrated that the ameliorative effect of LYC on aristolochic acid nephropathy was not due to the reduction of AAI intake by the kidney, but through the antioxidant, anti-inflammatory, and anti-apoptotic pathways demonstrated in this experiment. In order to investigate whether LYC has a therapeutic effect on AAN, we first performed in vivo experiments to verify the remission of renal injury in AAN mice after LYC intervention (including inflammatory response, oxidative stress injury, abnormal renal function, etc.). Demonstrated that LYC can be used as a protective agent to attenuate AAI-induced renal injury. The results showed that LYC could decrease the contents of Cr and BUN in the serum of AAN mice and inhibit the histopathological changes such as tubular injury, formation, inflammatory cell infiltration in the tubular epithelium. And LYC reduced collagen fiber accumulation in renal interstitium. In addition, the results of this study showed that LYC could significantly reduce the expression of NGAL and KIM-1 in the serum of AAN mice. KIM-1 is a transmembrane glycoprotein in renal proximal tubular epithelial cells that scavenges dead cells by recognizing phosphatidylserine and oxidized lipoproteins on the surface of dead cells [52]. KIM-1 and NGAL are minimally expressed at normal and significantly enhanced after kidney damage.

The body generates excessive ROS that can lead to cell damage and produce various effects, such as apoptosis, necrosis, and renal fibrosis [53]. Therefore inhibition of oxidative stress injury is key to improving

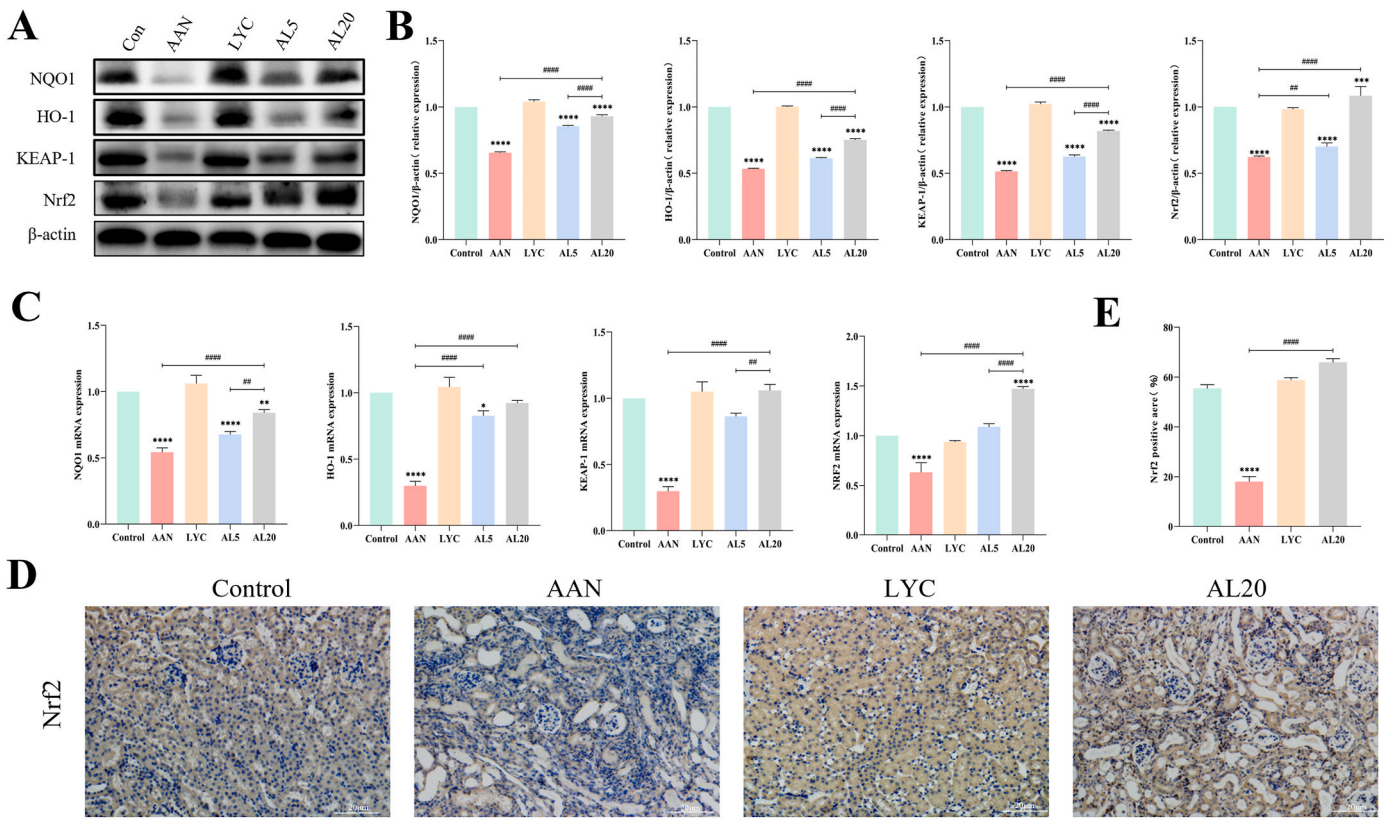

Fig. 12. LYC activated the Nrf2 antioxidant signaling pathway to alleviate AAI-induced oxidative stress in mice. A–C: Western-blot and RT-PCR detected the expression of NQO1, HO-1, Keap-1 and Nrf2. D: Representative image of immunohistochemical staining using anti-Nrf2 antibody. Scale bars were 50 μm. The percentage of positive regions for Nrf2 was quantified.

AKI and CKD. Nrf2 is a key transcription factor in the maintenance of oxidative homeostasis in cells [54] and is usually conserved in the cytoplasm by its inhibitor Kelch-like ECH-related protein 1 (Keap-1). Keap-1 undergoes a conformational change when cells are attacked by oxidative stressors. At this point, stable Nrf2 translocates to the nucleus and binds to antioxidant response elements (AREs) to initiate transcription of its downstream target genes [55]. Nrf2 activates the downstream HO-1/NQO1 antioxidant signaling pathway [56] with the aim of scavenging the body's excess ROS [57] and on antioxidant damage. In this study, both in vivo and in vitro results verified that LYC activated the nuclear translocation of Nrf2 to induce the expression of downstream target genes HO-1 and NQO1 and elevated the levels of antioxidant enzyme systems (GSH-PX, SOD, T-AOC). LYC reduced the accumulation of intracellular oxidative stress products (ROS, MDA) and ultimately alleviated oxidative stress damage. However, after NRK52E cells were treated with ML385, an inhibitor of Nrf2, antioxidant gene expression was decreased and a large amount of ROS accumulated intracellularly. This phenomenon was also unable to be reversed after the addition of LYC intervention. The Nrf2 activator AKBA was added to intervene the cells to further validate the mechanism of action of LYC. The results showed a consequent increase in antioxidant gene expression and scavenging of excess intracellular ROS. AKBA was consistent with the trend after LYC was applied to the cells. Together, these results indicated that LYC is able to activate the Nrf2 antioxidant signaling pathway and scavenge excess ROS from the body as well as ameliorate mitochondrial damage. Nrf2 is one of the main targets of LYC resistance to AAN.

Tumor necrosis factor-alpha (TNF-α) is a pleiotropic cytokine. It is activated to cause neurodegeneration, inflammation, autoimmune diseases, and cancer [58]. TNF-α is able to attract macrophages and T cells into the renal interstitium. Macrophages are the main cell type in maintaining the inflammatory response caused by a variety of endogenous cell injury factors [59]and are able to secrete inflammatory inducing cytokines (e.g. IL-1β, IL-6) [60,61]. Therefore, it has been previously demonstrated that TNF-α is key to trigger tubular epithelial cell necrosis, renal inflammation and fibrosis [62–64] and promotes the development of CKD [65]. It is known that accumulated ROS are able to activate TNF-α and stabilize its activity after the oxidative stress pathway is activated [66]. TNF-α can promotes the secretion of IL-1β in vivo [67]. In resting cells, NF-κB-p65 is inactivated by binding an inhibitory-κB (IκB) protein [17]. When the body suffers from endogenous stimuli (e.g. bacterial product TNFα or oxidative metabolite ROS), the stability of IkB is negatively controlled so that it exists in the form of phosphorylation [68]. After IkB is degraded by the proteasome, it leads to the release of NF-κB-p65 into the nucleus [69]. Subsequently p65 enhances NF-κB-related signaling pathway transduction cascades in a cell-specific manner [70] and ultimately activats the expression of inflammatory factors. The results of this study showed that AAI activated the expression of TNF-α, NF-κB-p65, and inflammatory factors (IL-1, IL-6, IL-1β) and inhibited the expression of IκB in tubular epithelial cells. LYC effectively inhibited the activation of TNF-α, the phosphorylation of NF-κB and the degradation of IκB. These results indicated that LYC improved inflammation in the kidneys of AAN mice mainly due to the inhibition of the TNF-α/NF-κB signaling pathway. However, the expression of NF-κ B and TNF-α was significantly increased after Nrf2 nuclear translocation was inhibited by ML385. Eventually, the inhibitory effect of LYC on the inflammatory response was alleviated. When the Nrf2 activator AKBA was added, the expression of NF-κB and TNF-α was again inhibited. The above results demonstrated that the activation of nuclear translocation of Nrf2 by LYC is a key factor in the inhibition of TNF-α/NF-κB signaling pathway. The transduction of the NF-κB inflammatory signaling pathway has been regulated by the Nrf2 antioxidant system.

Pathological apoptosis of renal tubular epithelial cells is able to

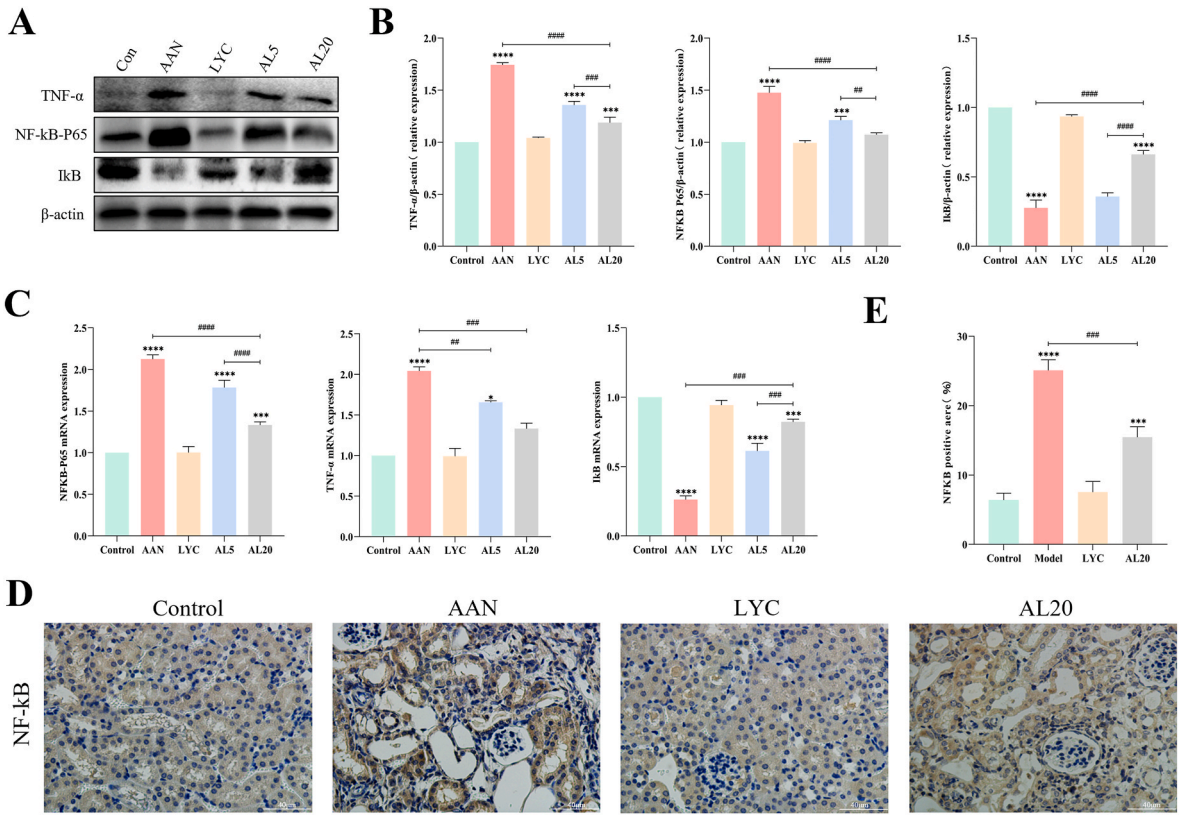

Fig. 13. LYC inhibited the NF-κB signaling pathway to inhibit AAI-induced inflammatory injury in the mouse kidney. A–C: Western-blot and RT-PCR detected expressions of TNF-α, NF-κB-p65 and IκB. D: Immunohistochemistry detected NF-kB-p65 expression. The percentage of positive regions for NF-κB was quantified.

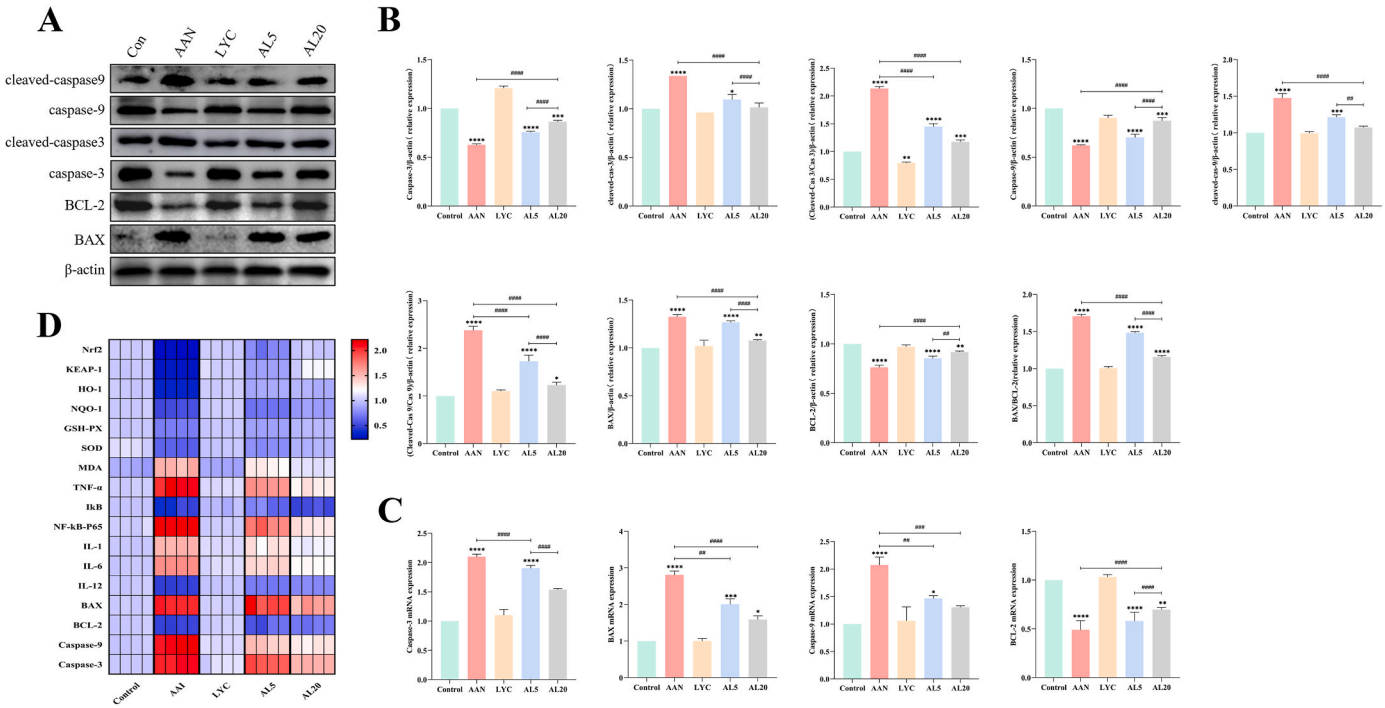

Fig. 14. LYC regulates apoptotic genes to inhibit AAI-induced apoptosis in mouse kidney cells. A, B: Western-blot detected expression of Cleaved- Caspase-9, Caspase-9, Cleaved- Caspase-3, Caspase-3, BCL-2 and BAX. C: RT-PCR analyzed the mRNA expression of BAX, Bcl-2, caspase-3, and caspase-9. D: Heat map of relative mRNA levels of Nrf2 system, NFKB signaling pathway, and apoptosis-related genes.

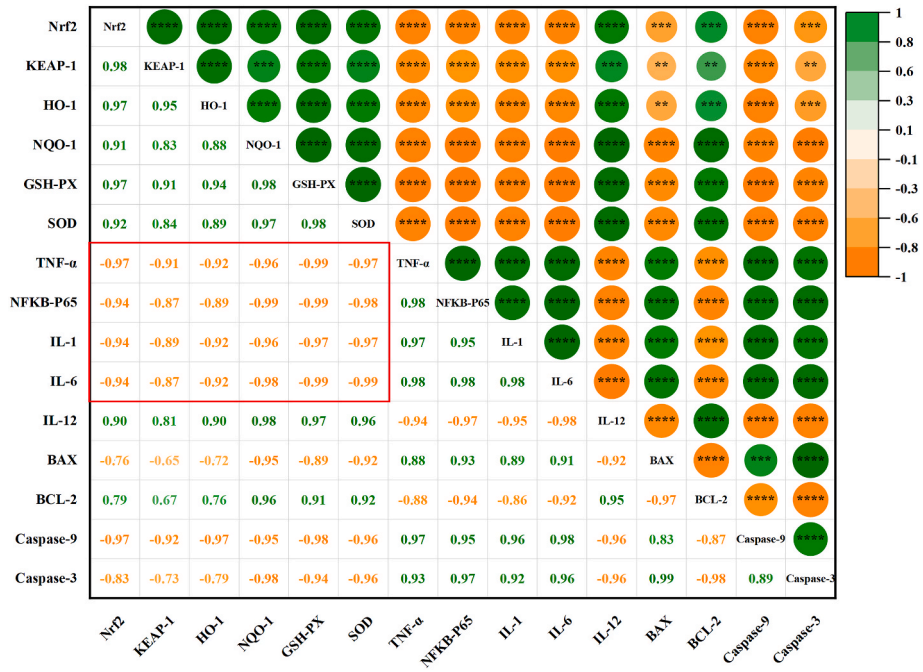

Fig. 15. Correlation analysis between NF-κB-related pathways, key factors of apoptosis and Nrf2 system. "Green" represented positive correlation and "yellow" represented negative correlation. * indicates $p < 0.05$, ** indicates $p < 0.01$, *** indicates $p < 0.001$ and **** indicates $p < 0.0001$. (For interpretation of the references to color in this figure legend, the reader is referred to the Web version of this article.)

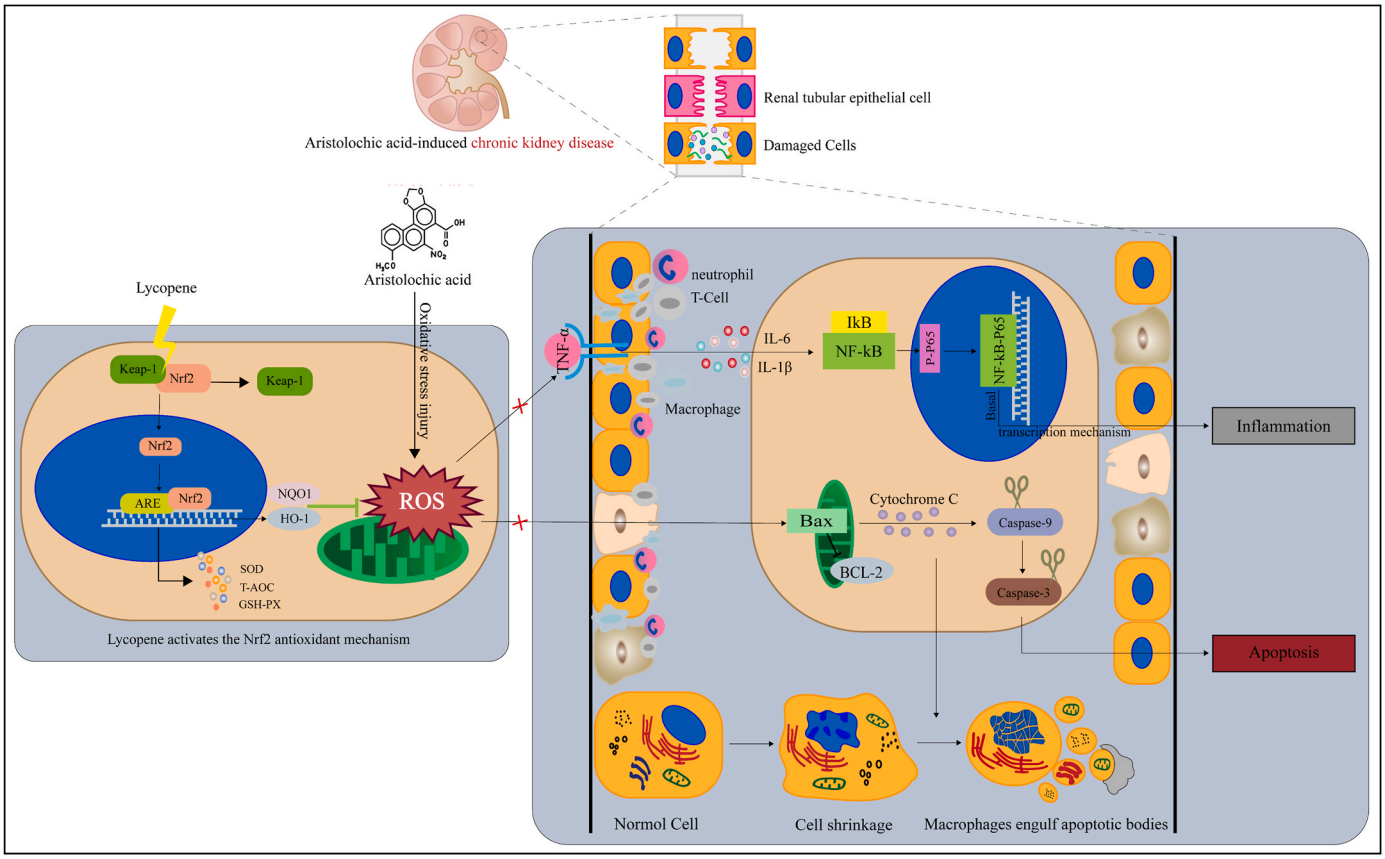

Fig. 16. Schematic diagram of the mechanism by which LYC improves AAN. LYC attenuated AAI-induced renal injury by regulating the antioxidant pathway of the Nrf2 system and inhibiting the activation of NF-κB signaling pathway and the occurrence of apoptosis.

exacerbate the development of chronic kidney disease [71]. As an organ with high energy demand, the kidney is second only to the heart in terms of mitochondrial mass and oxygen consumption [72]. Mitochondria are the major intracellular source of ROS [52,73]. ROS can lead to changes in mitochondrial inner membrane permeability [74,75]. ROS trigger apoptosis by activating the intrinsic mitochondrial pathway, the extrinsic death receptor pathway, and the endoplasmic reticulum (ER) stress pathway [76]. In this study, we observed renal tubular epithelial cells after AAI treatment by transmission electron microscopy. Mitochondria are the most severely damaged organelles. Mitochondria showed changes such as swelling, fragmentation, deformation, and dissolution. Preliminary results demonstrated that mitochondrial damage is one of the main pathogenesis causing AAN. The Bcl-2 protein family is a major effector of apoptosis. Among them, Bcl-2 is an anti-apoptotic gene, while BCL2-associated X protein (Bax) is a pro-apoptotic gene [3]. Oligomerization of BAX leads to outer membrane pore formation of mitochondria which in turn disrupts the membrane potential and leads to release cytochrome-c into cytosol [74]. Cytochrome-c is an important upstream regulator in apoptosis and is able to bind Pro-Caspase-9 to form "apoptosomes", ultimately leading to the activation of Caspase-9 [77]. Caspase-9 is a typical initiator of endogenous apoptosis triggered by mitochondrial damage. Caspase-9 is cleaved to induce the cleavage of downstream Caspase-3 [78] which further regulates the occurrence of apoptosis [79]. Mitochondrial damage is therefore an important factor leading to apoptosis. This study showed that LYC promoted the expression of BCL-2 and inhibited the expression of Bax, Cleaved-Caspase3 and Cleaved-Caspase9. The results of in vitro flow cytometry experiments showed that the number of apoptosis was significantly reduced after treatment with LYC. But the Nrf2 inhibitor ML385 activated the expression of pro-apoptotic genes again and inhibited the expression of Bcl-2. ML385 blocked the inhibitory effect of LYC on apoptosis. However, the addition of AKBA similarly inhibited apoptosis induced by AAI. Therefore, the above results demonstrated that LYC alleviated pathological apoptosis and mitochondrial damage induced by the BCL-2/Caspase family. This apoptosis pathway was regulated by the Nrf2 antioxidant system.

5. Conclusion

CONCLUSION: This study showed that LYC can ameliorate AAI-induced nephrotoxicity, which is associated with oxidative stress injury, inflammatory response and apoptosis. LYC alleviated mitochondrial damage and reduced the intracellular accumulation of ROS by activating the Nrf2/HO-1 antioxidant pathway. However, activation of the Nrf2 antioxidant system is a key factor in inhibiting TNF-α/NF-κB-induced inflammatory signaling pathways and apoptosis. Our data further supported the antioxidant mechanism of LYC and demonstrated that Nrf2 can be used as a research target for the treatment of such CKD. LYC has potential clinical applications as an intervention agent against AAN. (Schematic diagram of the mechanistic role of LYC in the treatment of AAN, Fig. 16).

Author contributions statement

Yu Wang: Data curation; Formal analysis; Writing. Zhihui Liu: Data curation. Jun Ma: Review. Qingyang Xv: Data curation. Hongxin Gao: Data curation. Hang Yin: Data curation. Ge Yan: Data curation. Wenhui Yu: Visualization; Funding acquisition; Review. Xiaowen Jiang: Visualization; Funding acquisition;

Declaration of competing interest

The authors declare that they have no known competing financial interests or personal relationships that could have appeared to influence the work reported in this paper.

Data availability

Data will be made available on request.

Acknowledgments

This study was financially supported by the National Natural Science Foundation of China (Grant No: 32072909).

Appendix A. Supplementary data

Supplementary data to this article can be found online at https://doi.org/10.1016/j.redox.2022.102494.

References

[1] J.Y. Kim, J. Leem, E.J. Jeon, Protective effects of melatonin against aristolochic acid-induced nephropathy in mice, Biomolecules 10 (1) (2019).
[2] R. Vanholder, et al., Biochemical and clinical impact of organic uremic retention solutes: a comprehensive update, Toxins 10 (1) (2018).
[3] C. Jin, et al., The renoprotective effect of diosgenin on aristolochic acid I-induced renal injury in rats: impact on apoptosis, mitochondrial dynamics and autophagy, Food Funct. 11 (9) (2020) 7456–7467.
[4] S. Wang, et al., Interleukin-22 attenuated renal tubular injury in aristolochic acid nephropathy via suppressing activation of NLRP3 inflammasome, Front. Immunol. 10 (2019) 2277.
[5] Q.B. Lu, et al., Salusin-β mediates tubular cell apoptosis in acute kidney injury: involvement of the PKC/ROS signaling pathway, Redox Biol. 30 (2020), 101411.
[6] A.A. Pozdzik, et al., Aristolochic acid induces proximal tubule apoptosis and epithelial to mesenchymal transformation, Kidney Int. 73 (5) (2008) 595–607.
[7] M. Sborchia, et al., The impact of p53 on aristolochic acid I-induced nephrotoxicity and DNA damage in vivo and in vitro, Arch. Toxicol. 93 (11) (2019) 3345–3366.
[8] J. Ren, et al., The transcription factor Twist1 in the distal nephron but not in macrophages propagates aristolochic acid nephropathy, Kidney Int. 97 (1) (2020) 119–129.
[9] J. Guo, et al., Isolevuglandins scavenger ameliorates myocardial ischemic injury by suppressing oxidative stress, apoptosis, and inflammation, Front. Cell Dev. Biol. 10 (2022), 836035.
[10] H. Sauer, M. Wartenberg, J. Hescheler, Reactive oxygen species as intracellular messengers during cell growth and differentiation, Cell. Physiol. Biochem. 11 (4) (2001) 173–186.
[11] H. Sies, D.P. Jones, Reactive oxygen species (ROS) as pleiotropic physiological signalling agents, Nat. Rev. Mol. Cell Biol. 21 (7) (2020) 363–383.
[12] J.D. Hayes, A.T. Dinkova-Kostova, K.D. Tew, Oxidative stress in cancer, Cancer Cell 38 (2) (2020) 167–197.
[13] H. Pelicano, D. Carney, P. Huang, ROS stress in cancer cells and therapeutic implications, Drug Resist. Updates 7 (2) (2004) 97–110.
[14] C. Chen, et al., Nrf2 deficiency aggravates the kidney injury induced by subacute cadmium exposure in mice, Arch. Toxicol. 95 (3) (2021) 883–893.
[15] B. Bellaver, et al., Hippocampal astrocyte cultures from adult and aged rats reproduce changes in glial functionality observed in the aging brain, Mol. Neurobiol. 54 (4) (2017) 2969–2985.
[16] S. Xie, et al., Andrographolide protects against adverse cardiac remodeling after myocardial infarction through enhancing Nrf2 signaling pathway, Int. J. Biol. Sci. 16 (1) (2020) 12–26.
[17] N.D. Perkins, Achieving transcriptional specificity with NF-kappa B, Int. J. Biochem. Cell Biol. 29 (12) (1997) 1433–1448.
[18] X. Song, et al., Recent trends and advances in the epidemiology, synergism, and delivery system of lycopene as an anti-cancer agent, Semin. Cancer Biol. 73 (2021) 331–346.
[19] N.E. El-Ashmawy, et al., Suppression of inducible nitric oxide synthase and tumor necrosis factor-alpha level by lycopene is comparable to methylprednisolone in acute pancreatitis, Dig. Liver Dis. 50 (6) (2018) 601–607.
[20] N. Gürbüz Çolak, et al., Mapping of quantitative trait loci for antioxidant molecules in tomato fruit: carotenoids, vitamins C and E, glutathione and phenolic acids, Plant Sci. 292 (2020), 110393.
[21] X.Y. Dai, et al., Lycopene attenuates di(2-ethylhexyl) phthalate-induced mitophagy in spleen by regulating the sirtuin3-mediated pathway, Food Funct. 12 (10) (2021) 4582–4590.
[22] J. Zhan, et al., Lycopene inhibits IL-1β-induced inflammation in mouse chondrocytes and mediates murine osteoarthritis, J. Cell Mol. Med. 25 (7) (2021) 3573–3584.
[23] J.E. Upritchard, W.H. Sutherland, J.I. Mann, Effect of supplementation with tomato juice, vitamin E, and vitamin C on LDL oxidation and products of inflammatory activity in type 2 diabetes, Diabetes Care 23 (6) (2000) 733–738.
[24] S. Zhou, et al., Inhibitory effect of lycopene against the growth of human gastric cancer cells, Afr. J. Tradit., Complementary Altern. Med. 13 (4) (2016) 184–190.
[25] T. Albrahim, M.A. Alonazi, Lycopene corrects metabolic syndrome and liver injury induced by high fat diet in obese rats through antioxidant, anti-inflammatory, antifibrotic pathways, Biomed. Pharmacother. 141 (2021), 111831.

[26] Y. Zhao, et al., Lycopene prevents DEHP-induced hepatic oxidative stress damage by crosstalk between AHR-Nrf2 pathway, Environ. Pollut. 285 (2021), 117080.
[27] L. Cui, et al., Anticancer effects and possible mechanisms of lycopene intervention on N-methylbenzylnitrosamine induced esophageal cancer in F344 rats based on PPARγ(1), Eur. J. Pharmacol. 881 (2020), 173230.
[28] Y. Zhao, et al., Lycopene prevents DEHP-induced liver lipid metabolism disorder by inhibiting the HIF-1α-Induced PPARα/PPARγ/FXR/LXR system, J. Agric. Food Chem. 68 (41) (2020) 11468–11479.
[29] D. Kong, et al., Curcumin blunts epithelial-mesenchymal transition of hepatocytes to alleviate hepatic fibrosis through regulating oxidative stress and autophagy, Redox Biol. 36 (2020), 101600.
[30] H. Li, et al., IL-23 reshapes kidney resident cell metabolism and promotes local kidney inflammation, J. Clin. Invest. 131 (12) (2021).
[31] H. Li, et al., Mst1 deletion attenuates renal ischaemia-reperfusion injury: the role of microtubule cytoskeleton dynamics, mitochondrial fission and the GSK3β-p53 signalling pathway, Redox Biol. 20 (2019) 261–274.
[32] Z.J. Fu, et al., HIF-1α-BNIP3-mediated mitophagy in tubular cells protects against renal ischemia/reperfusion injury, Redox Biol. 36 (2020), 101671.
[33] Y. Wang, et al., The PINK1/PARK2/optineurin pathway of mitophagy is activated for protection in septic acute kidney injury, Redox Biol. 38 (2021), 101767.
[34] J. Ge, et al., Comparative study on protective effect of different selenium sources against cadmium-induced nephrotoxicity via regulating the transcriptions of selenoproteome, Ecotoxicol. Environ. Saf. 215 (2021), 112135.
[35] X. Song, et al., Baicalin combats glutamate excitotoxicity via protecting glutamine synthetase from ROS-induced 20S proteasomal degradation, Redox Biol. 34 (2020), 101559.
[36] Q. Chi, et al., Roles of selenoprotein S in reactive oxygen species-dependent neutrophil extracellular trap formation induced by selenium-deficient arteritis, Redox Biol. 44 (2021), 102003.
[37] Y.J. Wang, et al., Induction of autophagy by pterostilbene contributes to the prevention of renal fibrosis via attenuating NLRP3 inflammasome activation and epithelial-mesenchymal transition, Front. Cell Dev. Biol. 8 (2020) 436.
[38] X.Q. Geng, et al., Ganoderic acid hinders renal fibrosis via suppressing the TGF-β/Smad and MAPK signaling pathways, Acta Pharmacol. Sin. 41 (5) (2020) 670–677.
[39] W. Dong, et al., Cadmium exposure induces rat proximal tubular cells injury via p62-dependent Nrf2 nucleus translocation mediated activation of AMPK/AKT/mTOR pathway, Ecotoxicol. Environ. Saf. 214 (2021), 112058.
[40] M. Liu, et al., Acetyl-11-keto-β-boswellic acid ameliorates renal interstitial fibrosis via Klotho/TGF-β/Smad signalling pathway, J. Cell Mol. Med. 22 (10) (2018) 4997–5007.
[41] X. Wang, et al., Upregulation of miR-382 contributes to renal fibrosis secondary to aristolochic acid-induced kidney injury via PTEN signaling pathway, Cell Death Dis. 11 (8) (2020) 620.
[42] V. Rudman-Melnick, et al., Single-cell profiling of AKI in a murine model reveals novel transcriptional signatures, profibrotic phenotype, and epithelial-to-stromal crosstalk, J. Am. Soc. Nephrol. 31 (12) (2020) 2793–2814.
[43] C. Pasten, et al., Aminoguanidine prevents the oxidative stress, inhibiting elements of inflammation, endothelial activation, mesenchymal markers, and confers a renoprotective effect in renal ischemia and reperfusion injury, Antioxidants 10 (11) (2021).
[44] J. Li, et al., The potential role of aquaporin 1 on aristolochic acid I induced epithelial mesenchymal transition on HK-2 cells, J. Cell. Physiol. 233 (6) (2018) 4919–4925.
[45] J.F. Chang, et al., Therapeutic targeting of aristolochic acid induced uremic toxin retention, SMAD 2/3 and JNK/ERK pathways in tubulointerstitial fibrosis: nephroprotective role of propolis in chronic kidney disease, Toxins 12 (6) (2020).
[46] H. Ding, Y. Xu, N. Jiang, Upregulation of miR-101a suppresses chronic renal fibrosis by regulating KDM3A via blockade of the YAP-TGF-β-smad signaling pathway, Mol. Ther. Nucleic Acids 19 (2020) 1276–1289.
[47] R. Samarakoon, et al., Loss of tumour suppressor PTEN expression in renal injury initiates SMAD3- and p53-dependent fibrotic responses, J. Pathol. 236 (4) (2015) 421–432.
[48] M.R. Littner, F.D. Lott, Increase in filtration coefficient from actions of melittin on neutrophils in isolated rabbit lungs, Am. J. Respir. Crit. Care Med. 149 (4 Pt 1) (1994) 867–872.
[49] A. Yefsah-Idres, et al., Hepatoprotective effects of lycopene on liver enzymes involved in methionine and xenobiotic metabolism in hyperhomocysteinemic rats, Food Funct. 7 (6) (2016) 2862–2869.
[50] C. Tong, et al., Intravenous administration of lycopene, a tomato extract, protects against myocardial ischemia-reperfusion injury, Nutrients 8 (3) (2016) 138.
[51] J.Y. Guo, et al., AQP2 as a target of lycopene protects against atrazine-induced renal ionic homeostasis disturbance, Food Funct. 12 (11) (2021) 4855–4863.
[52] D. Liu, et al., ROS-responsive chitosan-SS31 prodrug for AKI therapy via rapid distribution in the kidney and long-term retention in the renal tubule, Sci. Adv. 6 (41) (2020).
[53] D.O. Moon, et al., Butein induces G(2)/M phase arrest and apoptosis in human hepatoma cancer cells through ROS generation, Cancer Lett. 288 (2) (2010) 204–213.
[54] Z. Zhang, et al., Nrf2 antioxidant pathway suppresses Numb-mediated epithelial-mesenchymal transition during pulmonary fibrosis, Cell Death Dis. 9 (2) (2018) 83.
[55] T. Suzuki, M. Yamamoto, Molecular basis of the Keap1-Nrf2 system, Free Radic. Biol. Med. 88 (Pt B) (2015) 93–100.
[56] B. Xu, et al., Inhibition of PDE4 protects neurons against oxygen-glucose deprivation-induced endoplasmic reticulum stress through activation of the Nrf-2/HO-1 pathway, Redox Biol. 28 (2020), 101342.
[57] A. Khakurel, P.H. Park, Globular adiponectin protects hepatocytes from tunicamycin-induced cell death via modulation of the inflammasome and heme oxygenase-1 induction, Pharmacol. Res. 128 (2018) 231–243.
[58] C. Gao, et al., HSPA13 facilitates NF-κB-mediated transcription and attenuates cell death responses in TNFα signaling, Sci. Adv. 7 (41) (2021) eabh1756.
[59] C. Jin, et al., NLRP3 inflammasome plays a critical role in the pathogenesis of hydroxyapatite-associated arthropathy, Proc. Natl. Acad. Sci. U. S. A. 108 (36) (2011) 14867–14872.
[60] F. Yang, et al., c-Jun amino terminal kinase signaling promotes aristolochic acid-induced acute kidney injury, Front. Physiol. 12 (2021), 599114.
[61] M. Honarpisheh, et al., Aristolochic acid I determine the phenotype and activation of macrophages in acute and chronic kidney disease, Sci. Rep. 8 (1) (2018), 12169.
[62] Y.J. Ding, Y.H. Chen, Developmental nephrotoxicity of aristolochic acid in a zebrafish model, Toxicol. Appl. Pharmacol. 261 (1) (2012) 59–65.
[63] F.D. Debelle, et al., Aristolochic acids induce chronic renal failure with interstitial fibrosis in salt-depleted rats, J. Am. Soc. Nephrol. 13 (2) (2002) 431–436.
[64] S. Nlandu-Khodo, et al., Blocking TGF-β and β-catenin epithelial crosstalk exacerbates CKD, J. Am. Soc. Nephrol. 28 (12) (2017) 3490–3503.
[65] S. Rudloff, et al., Fetuin-A is a HIF target that safeguards tissue integrity during hypoxic stress, Nat. Commun. 12 (1) (2021) 549.
[66] J.N. Moloney, T.G. Cotter, ROS signalling in the biology of cancer, Semin. Cell Dev. Biol. 80 (2018) 50–64.
[67] T. Nakajo, et al., 1,25-Dihydroxyvitamin D(3) attenuates IL-1β secretion by suppressing NLRP1 inflammasome activation by upregulating the NRF2-HO-1 pathway in epidermal keratinocytes, Redox Biol. 48 (2021), 102203.
[68] V. Oliveira-Marques, et al., Role of hydrogen peroxide in NF-kappaB activation: from inducer to modulator, Antioxidants Redox Signal. 11 (9) (2009) 2223–2243.
[69] K. Jiang, et al., Therapeutic role of miR-30a in lipoteichoic acid-induced endometritis via targeting the MyD88/nox2/ROS signaling, Oxid. Med. Cell. Longev. 2021 (2021), 5042048.
[70] T. Zhang, et al., m(6)A mRNA modification maintains colonic epithelial cell homeostasis via NF-κB-mediated antiapoptotic pathway, Sci. Adv. 8 (12) (2022) eabl5723.
[71] Y. Li, et al., GSDME-mediated pyroptosis promotes inflammation and fibrosis in obstructive nephropathy, Cell Death Differ. 28 (8) (2021) 2333–2350.
[72] M. Zhao, et al., Mesenchymal stem cell-derived extracellular vesicles attenuate mitochondrial damage and inflammation by stabilizing mitochondrial DNA, ACS Nano 15 (1) (2021) 1519–1538.
[73] E.Y. Plotnikov, et al., The role of mitochondria in oxidative and nitrosative stress during ischemia/reperfusion in the rat kidney, Kidney Int. 72 (12) (2007) 1493–1502.
[74] S. Orrenius, V. Gogvadze, B. Zhivotovsky, Calcium and mitochondria in the regulation of cell death, Biochem. Biophys. Res. Commun. 460 (1) (2015) 72–81.
[75] J.L. Martin, et al., Mitochondrial mechanisms and therapeutics in ischaemia reperfusion injury, Pediatr. Nephrol. 34 (7) (2019) 1167–1174.
[76] M. Redza-Dutordoir, D.A. Averill-Bates, Activation of apoptosis signalling pathways by reactive oxygen species, Biochim. Biophys. Acta 1863 (12) (2016) 2977–2992.
[77] P. Li, et al., Cytochrome c and dATP-dependent formation of Apaf-1/caspase-9 complex initiates an apoptotic protease cascade, Cell 91 (4) (1997) 479–489.
[78] G. Groeger, C. Quiney, T.G. Cotter, Hydrogen peroxide as a cell-survival signaling molecule, Antioxidants Redox Signal. 11 (11) (2009) 2655–2671.
[79] T. Doke, et al., Genome-wide association studies identify the role of caspase-9 in kidney disease, Sci. Adv. 7 (45) (2021) eabi8051.
[80] Y. Guo, et al., Oral delivery of lycopene-loaded microemulsion for brain-targeting: preparation, characterization, pharmacokinetic evaluation and tissue distribution, Drug Deliv. 26 (1) (2019) 1191–1205.
[81] G.D. Marconi, et al., Ascorbic acid: a new player of epigenetic regulation in LPS-gingivalis treated human periodontal ligament stem cells, Oxid. Med. Cell. Longev. 2021 (2021), 6679708.
[82] W. Stuetz, et al., Plasma carotenoids, tocopherols, and retinol in the age-stratified (35-74 Years) general population: a cross-sectional study in six European countries, Nutrients 8 (10) (2016).